Spring 2017

Study of a High-Efficient Wide-Bandgap DC-DC Power Converter for Solar Power Integration

Yashwanth Bezawada
Old Dominion University

STUDY OF A HIGH-EFFICIENT WIDE-BANDGAP DC-DC POWER CONVERTER FOR SOLAR POWER INTEGRATION

by

Yashwanth Bezawada
B.Tech. May 2014, Malla Reddy Institute of Technology and Science, India

A Thesis Submitted to the Faculty of
Old Dominion University in Partial Fulfillment of the
Requirements for the Degree of

MASTER OF SCIENCE

ELECTRICAL AND COMPUTER ENGINEERING

OLD DOMINION UNIVERSITY

May 2017

Approved by:

Dr. Yucheng Zhang (Director)

Dr. Jiang Li (Member)

Dr. Shu Xiao (Member)

ABSTRACT

STUDY OF A HIGH-EFFICIENT WIDE-BANDGAP DC-DC POWER CONVERTER FOR SOLAR POWER INTEGRATION

Yashwanth Bezawada
Old Dominion University, 2017
Director: Dr. Yucheng Zhang

This research focuses on the design and analysis of a Boost cascaded Buck-Boost (BoCBB) power converter with super high efficiency in electric power conversion. The BoCBB power converter is based on emerging wide-bandgap silicon-carbide (SiC) MOSFETs and Schottky diodes, which have only 1/6 times of power loss in traditional silicon power semiconductor devices. The BoCBB power converter can be widely applied in solar harvesting for the National Aeronautics and Space Administration (NASA), military bases and electric utilities, as well as high-power DC motor drives for the electric vehicles, robotics, and manufacturing and product lines.

This research analyzed the topology and energy efficiency of a 3-kW BoCBB power converter. The energy efficiency of the SiC-based BoCBB power converter was calculated under various switching frequencies (20-kHz – 100-kHz) and was first tested by a simulation study of solar power integration in a 400-Vdc distribution microgrid in Matlab/Simulink environment. The design of 50-kHz in switching frequency revealed to be optimal in overall system performance. This conclusion was further verified by experimental tests. The experimental tests demonstrated a high efficiency of above 97% in power conversion. In order to improve the power quality of the BoCBB power converter for time-varying solar radiation, a novel sliding-window-combined (SWC) hysteresis control technique was proposed and preliminarily verified by a simulation study to enhance transients of a power grid.

This thesis is dedicated to my parents, my uncle, my family and my friends for providing me everything I need. It is also dedicated to my professor (Dr. Yucheng Zhang) for the support he provided throughout my thesis work.

ACKNOWLEDGMENTS

I express a whole hearted gratitude to Dr. Yucheng Zhang, Assistant Professor of Electrical and Computer Engineering, Old Dominion University for providing seamless support, guidance and knowledge throughout this thesis and also providing the right suggestions at every phase as development of my thesis.

I thank Dr. Shu Xiao, Associate Professor of Electrical and Computer Engineering, Old Dominion University for guiding me at the initial stage of my masters. His suggestions helped me academically and personally throughout the master's program.

I thank Dr. Jiang Li, Associate Professor of Electrical and Computer Engineering, Old Dominion University for being on my thesis committee and spending his valuable time for reviewing the thesis.

Special thanks to Dr. Dimitrie Popescu, Graduate Program Director of the Electrical and Computer Engineering department, Old Dominion University for his valuable suggestions since day one of my academic path, which helped me throughout my master's program.

I, gratefully acknowledge the support from the Air Force Civil Engineer Center (AFCEC) under Contract No. FA8051-15-C-0003. Any opinions, findings and conclusions or recommendations expressed in this material are of the author and do not necessarily reflect the views of the Air Force Civil Engineer Center (AFCEC).

Distribution A: Approved for public release; distribution unlimited. AFCEC-201724; 7 April 2017

NOMENCLATURE

BoCBB	Boost-Cascaded Buck-Boost
BoIBB	Boost-Interleaved Buck-Boost
BuCBB	Buck-Cascaded Buck-Boost
BuIBB	Buck-Interleaved Buck-Boost
CCM	Continuous Conduction Mode
CV	Constant Voltage
DC-DC	Direct Current to Direct Current
DOE	Design of ExperimentS
FL	Fuzzy logic
GW	Gigawatts
IC	Incremental Conductance
MPPT	Maximum Power Point Tracking
MPP	Maximum Power Point
OCV	Open Circuit Voltage
PCB	Printed Circuit Board
PD	Proportional-Derivative
PI	Proportional-Integral
PID	Proportional-Integral-Derivative
PV	Photovoltaic
PWM	Pulse Width Modulation
RES	Renewable Energy Sources

SCP	Short Current Pulse
Si	Silicon
SiC	Silicon Carbide
SWC	Sliding-Window-Combined
TSBB	Two Switching Buck-Boost

TABLE OF CONTENTS

LIST OF TABLES

LIST OF FIGURES

Figure Page

CHAPTER 1
INTRODUCTION

1.1 Introduction

Fossil fuels such as coal and oil, have been used very often for the supply chain. But due to the increase in population, the requirement of the energy supply has increased and exposed the limitations of these fuels. Even though fossil fuels are easy to extract, they are depleting, limited, and unsustainable in the longer term. Other than limitations, pollution is a major disadvantage of fossil fuels. They release carbon dioxide when burned thereby determining the greenhouse effect. Extraction of coal results in the destruction of wide areas of land and extracting coal is considered a high risk activity. All of these disadvantages of fossil fuels develop great interest in renewable energy sources (RES). Among RES, solar energy can easily be deployed by both home and commercial power users as it does not require any huge setup.

Solar energy is a widely available energy resource on earth. The amount of solar energy strikes on earth (173,000 Tera watts) is 10,000 times the world's total energy use [1]. In the past eight years, the amount of solar power installed in the U.S has increased more than 23 times. According to a solar industry update, the United States has installed 4.0 gigawatts (GW) in the first half of 2016, which is a 47% increase compared to the first half of 2015. It is estimated that by the end of 2016, about 61 GW to 74 GW of photovoltaic (PV) will be installed globally [1]. With the increase in demand and number of installations, analysts have reported a significant drop in PV module pricing. As mentioned, the use of solar energy has resulted in substantial environmental and human health benefits. A recent design of experiments of a U.S study states that, in 2014, solar power saved 17 metric tons of carbon dioxide. The study also states that 7.6 billion gallons of water consumption has been reduced from the power sector [1].

PV cells are used to convert solar energy into electric energy. When a semiconductor device is exposed to light, the photons of the light ray are absorbed by the semiconductor crystals, which releases free electrons. These free electrons are the reason for the production of electricity.

1.2 Characteristics of Photovoltaic Cell

Fig 1 shows the equivalent circuit of PV cell. PV cells can be modeled as current source in parallel with a diode and behave like a diode since current source acts like open circuit when no light strikes on the surface of the PV cell [2].

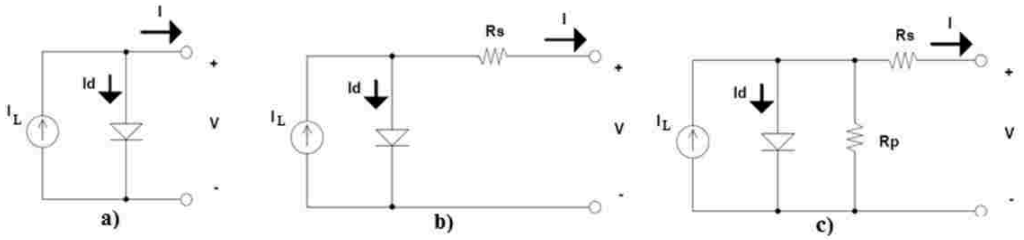

Fig 1. The equivalent circuit of a PV cell

In [2], by applying Kirchhoff's Law for an ideal PV cell I_{ph}, the PV current is equal to the current generated by photoelectric effect minus the diode current I_d.

$$I_{ph} = I - I_d \tag{1}$$

where I_d is proportional to the saturation current given by

$$I_d = I_o \left[exp\left(\frac{V}{A.N_S.V_T}\right) - 1\right] \tag{2}$$

V is the voltage imposed in the diode.

$$V_T = \frac{\text{k..}T_c}{\text{q}} \tag{3}$$

where, I_0 = reverse saturation or leakage current of the diode (A).

V_{Tc} = 26 mV at 300 K for silisium cell (V).

K = Boltzmann constant ($1.381*10^{-23}$ J/K).

q = electron charge (1.602×10^{-19} C).

V_T = thermal voltage (V).

Ns = number of PV cells connected in series (no units).

A = ideality factor (no units).

Considering the series resistance R_S and parallel resistance R_P, the diode current gives

$$I_d = I_o[\exp(\frac{V+I.R_S}{a})\text{-}1] \quad (4)$$

By applying the Kirchhoff's Law,

$$I = I_{ph} - I_d - I_p \quad (5)$$

$$I = Iph - I_o\left[\exp\left(\frac{V+I.R_S}{a}\right) - 1\right] - \frac{V+R_S.I}{R_p} \quad (6)$$

Based on the equations (1) to (6) and considering the environment parameters G = 200, 400, 600, 800 and 1000 (W/m2), and T = 0, 10, 20, 30, 40 and 50 (Celsius), Fig 2 shows typical I-V relationships for a PV module under various irradiance. This graph also plots the power output (P) for the PV module. From these plots, it can be observed that there is a point at which the power produced by the PV module is at its maximum value; this corresponds to the knee point of the V-I curve. An important capability for any effective PV application is the ability to dynamically track this point under varying irradiance. For solar power extraction for medium scale or large scale systems, two traction methods are used i.e. sun tracking and the Maximum Power Point Tracking (MPPT).

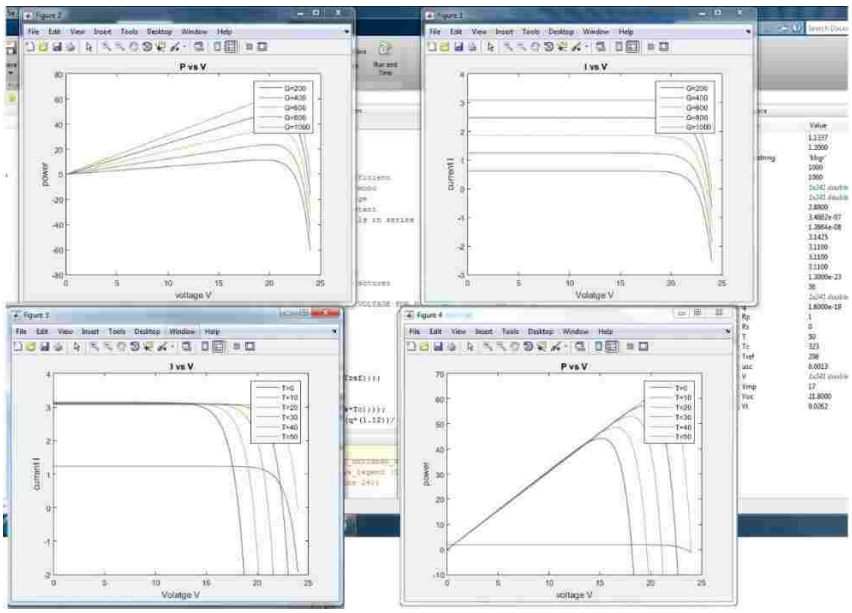

Fig 2. P-V and I-V characteristics of Photovoltaic cell

1.3 Maximum Power Point Tracking (MPPT)

The MPPT technique is used to extract the maximum power at any given environmental condition. Technically MPPT technique is generally applied for PV solar systems and wind turbines. MPPT tackles the efficiency of power transfer from the PV cell depending on the amount of sunlight on the solar panels and the electrical characteristics of the load i.e. the output voltage of PV cell.

The efficiency of the solar power system is optimized for varying load characteristics to keep the maximum power transfer at high efficiency. Solar cells have a complex relation between temperature and irradiance that produces a non-linear output efficiency which can be analyzed based on I-V curve [3]. MPPT controller are tuned as power converters to control the voltage and current conversation that sample the output of the PV cells [4].

Nineteen distinct MPPT methods have been proposed by peer researchers, which are summarized in [5]. In the CV method, MPPT is achieved by considering reference voltage value (V_{ref}) under a varying conditions. Although the CV method is simple and inexpensive to implement, it is not flexible under dynamically varying operating conditions. But under the low irradiance conditions, the algorithm of the CV method has proven to be more effective than others. For this reason, the CV method can be combined with other MPPT techniques [6].

Open circuit voltage (OCV) is a technique similar to the CV method, periodically open circuits the PV array. The OCV method is efficient to compensate temperature effect, which affects the output voltage of the PV cell. The set point of PV voltage is determined as a certain percentage of V_{OC}, typically between 71-78%; there is no power generated at the downside when PV array is in open circuit [5]. The drawback of this method is it can only approximate the maximum power point.

Short current pulse (SCP) is another MPPT technique similar to OCV. In the SCP technique, the PV panel is short-circuited rather than open-circuited. The solar power converter is regulated by a current control loop and the operating current is commanded to be a percentage of the I_{SC}, often around 92% [6]. Since I_{SC} is dependent on irradiance, it is comparatively insensitive to temperature and no power is

generated, while the PV array is being short circuited. The SCP method is more effective to varying irradiance compared to differences in the PV module temperature.

Other than the OC, OCV, and SCP methods, there are other methods which can be used to determine the true maximum power point. Extremum-seeking control theory uses a feedback system to induce oscillations around the equilibrium point to realize maximum power point [7]. The Perturb-and-Observe (P&O) method periodically adjusts the operating point and measures the instantaneous solar power output. The solar power converter will adjusts the operating point in the same direction when the solar power increases. The operating point reverses its direction when the solar power gets decreased. Although this method is effective, it may not be able to take care of frequent changes in environmental conditions since it would oscillate around the maximum power point [6].

The incremental conductance (IC) methods eliminates the oscillations around the output, which improves the P&O method. To achieve the maximum power point, the IC method forms a connection between the instantaneous conductance (I/V) and incremental conductance ($\frac{dv}{dt}$) values to calculate both the magnitude and direction. Both P&O and IC may make use of fuzzy logic to increase performance and accuracy [6] [7].

1.4 Previous Research of Solar Power Converters

DC-DC power converters play an important role in the PV interface system. The function of the DC-DC power converter is to maintain the output voltage and to achieve the MPPT with the use of voltage/power control techniques. Previously, peer researchers used isolated DC-DC power converters like Flyback and Push-Pull as a power converter for the PV interface system. An isolated DC-DC power converter contains power transformers to isolate input power to the output power. A power transformer can be used to transfer high voltages and to provide galvanic isolation, improve safety, and enhance noise immunity.

Besides these advantages, isolated DC-DC power converters also have the following drawbacks, like size, and cost, as well as low efficiency and additive heat dissipation, which are the essential impacts

in field applications. Therefore, this leads to the interest of non-isolated DC-DC power converter like Buck, Boost, and Buck-Boost power converters. These power converters are most frequently used nowadays for PV interface system. A Boost power converter is commonly used as a non-isolated DC-DC power converter in order to step up PV voltage as well as to achieve MPPT. The block diagram of conventional PV grid connection is shown in Fig 3. Several methods has been implemented to achieve high voltage gain for the Boost power converter.

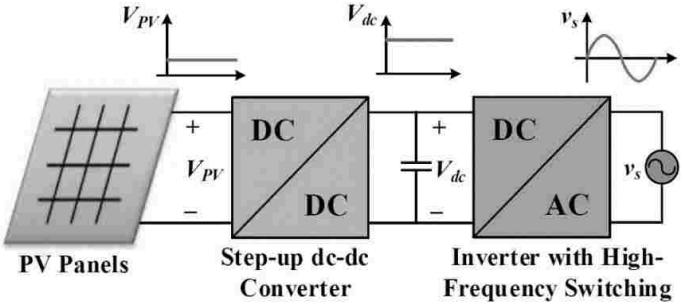

Fig 3. The block diagram of conventional PV grid connection system

But PV voltages vary widely due to changes in temperature and irradiance. For this case depending on the voltage level, step up function along with a step down function is needed for a DC-DC power converter. Although a traditional Buck-Boost power converter can be operated in these functions, but in a traditional Buck-Boost power converter, the entire energy gets stores in an inductor which imposes current stress and low conversion efficiency [8]. Individual Buck and Boost power converters impose low voltage stress on elements compared to the Buck-Boost power converter. The use of Buck and Boost power converters allows to connect the direct path between the output and input, which leads to the maximum energy transfer due to low voltage stress.

Several multi-stage DC-DC power converters have been proposed to provide high voltage gains, and to reduce voltage stress across circuit components as well as high efficiency. Parallel, cascading, and Interleave are types of multi-stage DC-DC power converters. Various interleaved power converters are proposed such as Bidirectional interleaved DC-DC power converters [9], interleaved couple inductor Boost

power converters [10] and interleaved Boost DC-DC power converters [11]. The major advantage of these interleaved power converters is that they all can achieve a very low ripple current in the source. Alongside the fact that the current stress and filter size of these power converters are low, these power converters can only perform voltage step-up operations. These limitations in the previous research lead to two-switching Buck-Boost power converters. Boost Cascaded Buck-Boost (BoCBB) power converter is among the proposed two switch Buck-Boost (TSBB) DC-DC power converters applicable for the current design.

A DC-DC power converter generates a transient response whenever the change in mode takes place i.e. Buck to Boost mode or vice versa. The number of transient responses can be controlled by an operating circuit by using a hysteresis controller. Several control techniques have been used earlier in order to achieve better performance and stability of a designed system. [12] discussed the design and implementation issue, and the experimental results of the linear PID and PI controller and fuzzy controller were compared. The design of linear PID and PI controllers and fuzzy controllers requires quite different procedures. The design of the fuzzy controller does not require a mathematical model but, comparatively, a small signal model is needed for the design of PID controllers. But the disadvantage of the above method is the implementation of fuzzy controllers demands more computation power and memory than implementation of linear controllers.

In [13], the formulation of a PID controller is introduced to replace the output voltage derivative with the information of the capacitor current. In this way, the noise injection is reduced. This formulation preserves the fundamental principle of a PID controller and incorporates a load current feed forward as well as inductor current dynamics. The drawback of the method is the derivative gain never changes, even at switching transition. Therefore, impulse noise injection due the derivative term of a conventional PID control is avoided by using the proposed PID formulation. [14] discusses the use of Internal Model Control and Model Reference Control structures of Posicast-based control scheme which is applicable to parameter uncertain plants. This method still needs more investigation on its stability during transients. These drawbacks in the previous research leads to implementation of a hysteresis controller to reduce the number

of transient responses. In this thesis, a sliding-window combined (SWC) hysteresis control technique is discussed more in details in Chapter 3.

1.5 Objective of this Project

The aim of the thesis is to design, test, and analyze the Boost-Cascaded Buck-Boost (BoCBB) DC-DC power converter used for PV power system applications. The BoCBB DC-DC power converter proposed in this thesis can fit commercial PV power systems utilized in the military, NASA, robotics, and automobiles. Implementation of MPPT method is used as a part of power converter design in order to extract maximum power. The efficiency of the BoCBB power converter under various switching frequency has been found by using a calculation of power losses in the circuit. Testing of BoCBB is performed by using Matlab/Simulink software. The experiment is performed to validate the theoretical analysis of efficiency analysis of the BoCBB DC-DC power converter.

A BoCBB power converter is considered as a DC-DC power converter for the PV interface. BoCBB has potential to tackle varying PV voltages and has the advantage of low voltage stress on components compared to other multi-stage DC-DC power converters. Alongside performing both step-up and step-down functions, efficiency of the DC-DC power converter is also one of the major considerations in this thesis. The selection of components such as power semiconductor switches, diodes, and inductors plays an important role in high-efficient power converter design. In this project, emerging SiC material MOSFETs and Schottky diodes are adopted to reduce the power losses at the switching and conduction losses, which improves the efficiency of the circuit. Simulations are performed by using PI controller to achieve MPPT. Also switching modes in BoCBB leads to transient response. The PV characteristics are non-linear varying in temperature and irradiance, which leads to frequent transient responses in the system, reducing the number of transients by operating the BoCBB with the help of a novel sliding window technique. Hysteresis controllers are implemented and compared to reveal the benefits of a sliding window concept for BoCBB. The hardware implementation of BoCBB considers the CREE MOSFET's driver circuit in order to achieve faster switching.

1.6 Thesis Outline

Chapter 1 explores the reasons of developing solar energy to replace traditional fossil fuels. The amount of solar energy installation in the United States during 2015 and 2016 and its estimation of near future have been discussed. Photovoltaic characteristics of the solar cell has been shown for different temperatures and irradiance. The concept of MPPT as well as several MPPT techniques have been introduced. Also introduced a various DC-DC power converters used in the earlier of stage to achieve MPPT.

Chapter 2 discusses the types of multistage Buck-Boost power converters implemented and detailed explanation of the reasons for using a Boost Cascaded Buck-Boost power converter (BoCBB). The parameters of 3kW and 400V output voltage of BoCBB are specified. The controller part of BoCBB is explained by using two flow charts for both Buck and Boost mode. Separately, efficiency of energy conversion in BoCBB by using SiC and Si MOSFET is compared by using the power losses calculations of the MOSFET, Schottky diode, and inductor.

Chapter 3 analyses the control part of the BoCBB. The chapter introduces controller topologies with the circuit diagrams and explains about the drawbacks of them in detail. This chapter focuses on the design of the SWC hysteresis controller. By using simulation results, the decrease in number of modes by using sliding window controller has been explained.

Chapter 4 describes the simulation design and analysis of the BoCBB DC-DC power converter. The simulation results are presented. Also, the PCB design of the BoCBB and its driver circuit for CREE SiC MOSFET are explained in detailed with the operation.

Chapter 5 exhibits the hardware test results of the BoCBB without controller topology by considering several duty cycle values. Performance of CLC filter for 20kHz, 50kHz and 100kHz is presented in this chapter.

Chapter 6 concludes the 50kHz switch frequency as an optimal frequency for the SiC based BoCBB power converters and future work on BoCBB is proposed in this chapter.

CHAPTER 2

BOOST-CASCADED BUCK-BOOST POWER CONVERTER

2.1 Introduction

In Chapter 1, several multi-staging techniques were mentioned. This chapter introduces several TSBB power converters. These power converters can be operated in both Buck and Boost modes based on varying PV voltage. Multi-stage DC-DC power converters can achieve high gain and high efficiency. When power converters are cascaded, the output of the first stage becomes the input for the second stage. Conventional Buck-Boost power converters store all energy in the inductor and then delivers to the output which suffers from high inductor current stress and low conversion efficiency [15]. The TSBB DC-DC power converters are proposed to solve the reverse output voltage problem. When two switches of TSBB DC-DC power converters operate with two independent control and non-simultaneous switching, the TSBB DC-DC power converters will function as either Buck power converters or Boost power converters. Therefore, partial energy can be directly delivered to the output, which leads to higher efficiency [16] [17].

2.2 Types of TSBB DC-DC Power Converters

Several TSBB DC-DC power converters have been proposed [18] which includes Buck-Cascaded Buck-Boost (BuCBB) DC-DC power converters, Boost-Cascaded Buck-Boost (BoCBB) DC-DC power converters, Buck-Interleaved Buck-Boost (BuIBB) DC-DC power converters, and Boost-Interleaved Buck-Boost (BoIBB) DC-DC power converters, as shown in Fig 4.

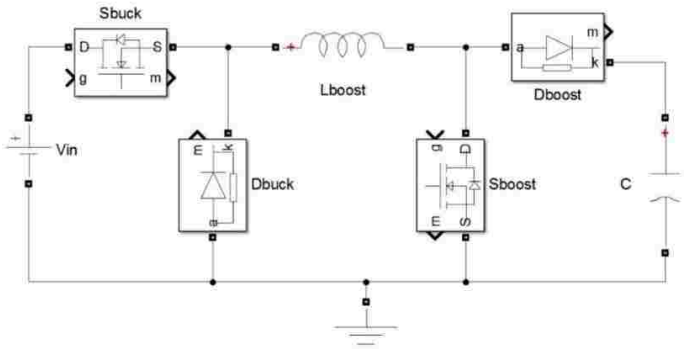

a) Buck-Cascaded Buck-Boost power converter

Fig 4. TSBB DC-DC power converters

Fig 4. (Cont.)

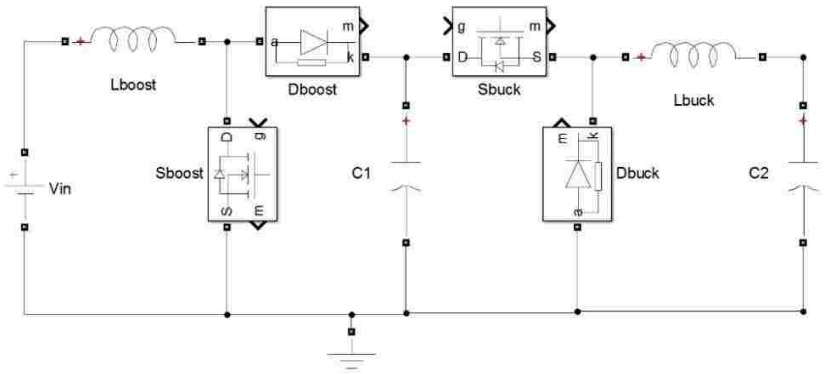

b) Boost-Cascaded Buck-Boost power converter

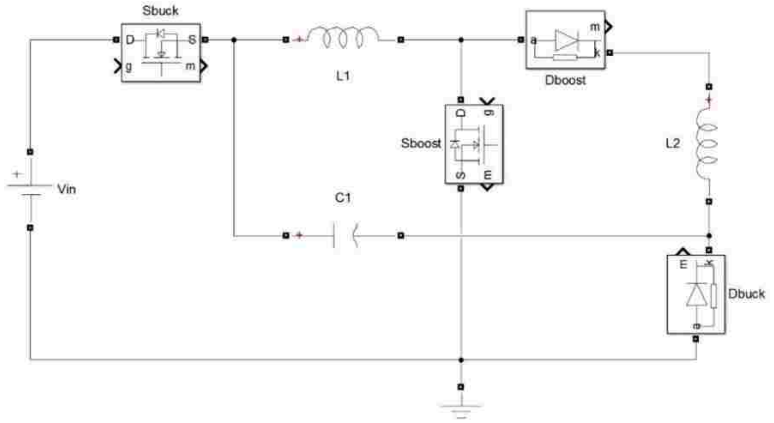

c) Buck-Interleaved Buck-Boost power converter

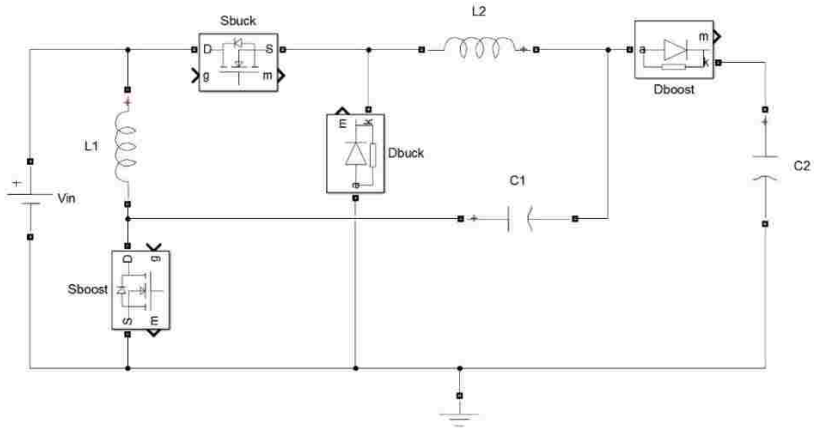

d) Boost-Interleaved Buck-Boost power converter

The BoCBB power converter has the simplest circuit among the proposed TSBB DC-DC power converters. As discussed above, S_{Boost} and S_{Buck} switches are operated independently to deliver energy directly. As shown in Table 1, the inductor L1 acts as Boost inductor and L2 act as a filter when BoCBB is in Boost mode. For the Buck mode inductor L1 acts as filter and L2 acts as Buck inductor when BoCBB is in Buck mode. In order to pass low frequency energy, the inductor is required at the input of the proposed TSBB DC-DC power converters. BoCBB is considered to be more suitable for this case.

Table 1: Inductor functionality in TSBB power converters

Mode/ Topology	L1		L2	
	Buck	Boost	Buck	Boost
BuCBB	Buck Inductor	Boost Inductor	N/A	N/A
BoCBB	Filter	Boost Inductor	Buck Inductor	Filter
BuIBB	Buck Inductor	Boost Inductor	Buck Inductor	Filter
BoIBB	Filter	Boost Inductor	Buck Inductor	Boost Inductor

2.3 Specification of a 3kW BoCBB DC-DC Power Converter

BoCBB acts as a Boost power converter for the low input voltages and a Buck power converter for the high input voltages (as discussed, input voltage depends on the temperature and irradiance).A traditional Buck-Boost power converter cannot be directly used for this case because of the poor switch utilization, achieving a maximum of 25% at a duty ratio of 50%, when $V_{in} = V_{out}$ (for Continuous Conduction Mode, CCM) [19].

Specifications of BoCBB DC-DC power converter are shown below

Power rating = 3KW

Input voltage = [300V- 480V]

Output voltage = 400V

Switching Frequency = 20kHz , 50kHz, and 100kHz

Calculations of components value in Boost cascaded Buck-Boost (BoCBB) power converter are shown in Equations (7)-(10).

$$L_{Boost} = \frac{V_g}{2\Delta i_L} DT_s \quad (7)$$

$$C_{Boost} = \frac{V}{2R\Delta V} DT_s \quad (8)$$

$$L_{Buck} = \frac{(V_g - V)}{2\Delta i_L} DT_s \quad (9)$$

$$C_{out} = \frac{\Delta i_L}{8\Delta V_{out}} T_s \quad (10)$$

By using the above equations the component values of BoCBB is shown in Table.2

Table 2: Component values of BoCBB circuit

	Buck mode	Boost mode
V_{in}	480V	300V
L1	5.6 mH	5.6 mH
L2	4.4 mH	4.4 mH
C1	100 nF	100 nF
C2	50 µF	50 µF
R_{load}	53.3 Ω	53.3 Ω
V_{out}	400V	400V

2.4 Switching Operation of BoCBB

A switching operation is performed according to the varying input voltage V_{in}. S_{Boost} and S_{Buck} are operated independently. When BoCBB is in Buck mode, the duty cycle of S_{Buck} will be D = $\frac{\text{Vout}}{\text{Vin}}$ which adjusts the width of the pulse signal and S_{Boost} will be in off state i.e. open circuit as shown in Fig 5.When BoCBB is in Boost mode, the duty cycle D = 1- $\frac{V_{in}}{V_{out}}$ of the pulse signal is adjusted according to varying input. This pulse signal is given to the S_{Boost}. In order to pass the voltage to the load S_{Buck} should be short circuited i.e. S_{Buck} should be always turned on (S_{Buck} =1), as shown in Fig 6.

When $V_{in} > V_{out}$

$$S_{Boost} = 0 \tag{11}$$

$$\text{Duty cycle D} = \text{SBuck} = \frac{\text{Vout}}{\text{Vin}} \tag{12}$$

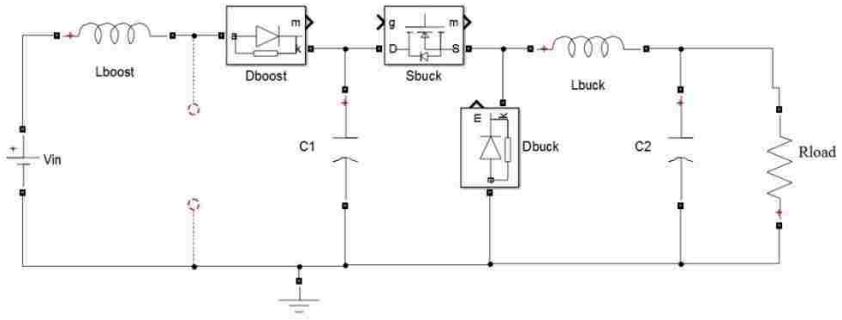

Fig 5. BoCBB power converter in Buck mode

When $V_{in} <= V_{out}$

$$\text{Duty cycle D'} = \text{SBoost} = 1 - \frac{Vin}{Vout} \tag{13}$$

$$S_{Buck} = 1 \tag{14}$$

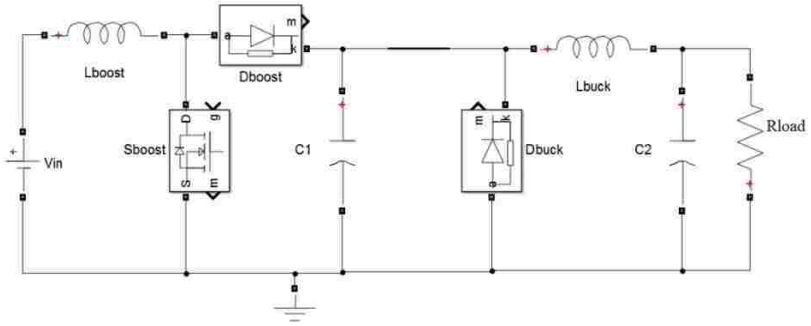

Fig 6. BoCBB power converter in Boost mode

2.5 Power Losses Analysis

The total power dissipated by the DC-DC power converter is calculated by the summation of power losses at each power component. Control circuitry and inductor losses are least dependent on input power.

The maximum efficiency depends on selection of power components. A BoCBB power converter's power losses are associated with MOSFET, Schottky diode, and the inductor. A major contribution of the power losses comes from the MOSFET. Conduction losses of MOSFET are higher than the switching losses because of high channel resistance and low gate charge.

2.5.1 Losses associated with MOSFET

In this case, MOSFETs are used as a switch for the BoCBB, since MOSFETs can be used for long duty cycles, variation in the loads, and for high frequencies. Typically, MOSFETs are associated with conduction losses and switching losses. The majority of the power losses in the circuit are due to conduction and switching in the MOSFETs. Since the BoCBB power converter has high side and low side switching, the power losses are calculated for both sides individually depending on the Buck mode or Boost mode.

$$P_{MOSFET} = P_{Swit,\ losses} + P_{cond,\ losses} \quad (15)$$

High side conduction losses:

$$P_{cond(hs)} = I_{out}^2.R_{DS(ON)}.D \quad (16)$$

High side switching losses:

$$P_{swit(hs)} = \frac{I_{out}.V_{in}}{2}.\left(t_{rise} + t_{fall}\right).F_{Sw} \quad (17)$$

Low side conduction losses:

$$P_{cond(ls)} = (1- D).I_{out}^2.R_{DS(ON)} \quad (18)$$

Low side switching losses:

$$P_{swit(ls)} = \left(\frac{V_F+I_{out}.1.1.R_{DS(on)}}{2}.t_{rise} + t_{fall}.V_F\right) I_{out}.F_{Sw} \quad (19)$$

Low side switching losses are very small. It can be ignored while calculating total losses.

Whereas $D = V_{out}/V_{in}$ for Buck power converter

$D = V_{in}/V_{out}$ for Boost power converter

I_{out} = output current

F_{SW} = Switching Frequency

R_{DS} = Source to drain resistance, t_{rise}(rise time), t_{fall}(fall time), V_F(Forward voltage drop) is given by the manufacturer.

2.5.2 Diode losses

The power losses in the diode are determined based on forward voltage, V_F. A Schottky diode should be used whenever possible since it has a low forward voltage (~ 0.3V) and minimal reverse recovery time.

$$P_{DIODE} = (1\text{-}D).V_F.I_{out} \quad (20)$$

2.5.3 Inductor Losses

The power losses in the inductor can be seen in the hysteresis curve. Hysteresis is one of the core-material characteristics that causes power loss in the inductor core. Two types of losses are present in the inductor 1) core losses and 2) low frequency copper losses [20]. Fig 7 shows the hysteresis curve of power inductor. The variation zone of B and H in this research has been marked as dB and dH in a traditional B-H curve of electrical magnetic material, as indicated in Fig 7. This curve is used to find the ΔB (i.e. dB) which determines the core losses.

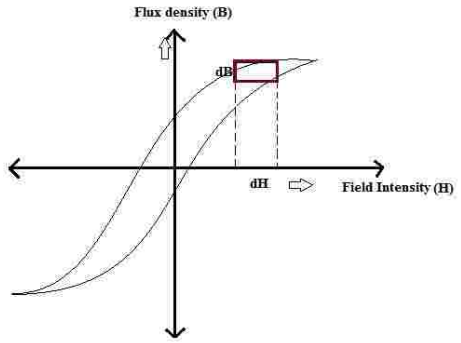

Fig 7. Hysteresis (B-H) curve of power inductor

Core losses and Copper losses or eddy losses:

Core losses depends on the core used. Usually for an inductor, iron alloys are used as a core, which is a good conductor of electricity, therefore it produce an eddy current in the core. According to Faraday's law,

the AC flux induced voltage in the core is proportional to the derivative of the flux. The voltage magnitude increases directly with the excitation frequency, f. When the impedance of the core material is purely resistive, it will be independent of frequency. The magnitude of the induced eddy currents increases directly with f^2. This implies that the eddy current losses should increase as frequency increases [20].

High operating flux density leads to reduced size, weight, and cost. Silicon steel and similar materials exhibit saturation flux densities of 1.5 to 2 T, but it exhibits high core losses. In case of low resistive materials the eddy losses will be high [20]. The core losses can be written as

$$P_{fe} = k_{fe}.(\Delta B)^{\beta}.A_c.l_m \quad (21)$$

whereas A_c = Area of the core (cm)

$$\Delta B = \frac{T.D.(V_g)}{N.A_c} \text{ \{for Boost power converter\}}$$

$$\Delta B = \frac{T.D.(V_g - V_{in})}{N.A_c} \text{ (T) \{for Buck power converter\}}$$

D is duty cycle (no units)

β = 2.7 (no units) (decided by the manufacturer, usually lies in between 2.6 to 2.8)

k_{fe} (cm^x)and l_m (cm) is decided by the manufacturer

For this case EER cores are used for the inductor, based on LI^2 and A_L values type of the EER core can be selected. By using L= 5.6mH and I= 7.5A, A_L =650mH/1000 turns.

By using L and A_L

$$N = 10^3 \sqrt{\frac{L}{A_L}} \quad (22)$$

N = 93 turns

Here, EER40 is used as a core based on $L.i^2$. By looking at Appendix D in [20], l_m (magnetic path length), k_{fe}(constant), A_c (cross sectional area), MLT (mean length per turn), W_A(winding area) can be determined.

$$P_{copper} = I^2.R_{ac} \quad (23)$$

$$R_{ac} = \frac{h}{\delta} R_{dc} \quad (24)$$

$$\delta = \frac{7.5}{\sqrt{f}} \tag{25}$$

$$R_{dc} = \rho \frac{N l_m}{A_w} \tag{26}$$

N = number of turns (no units)

f = switching frequency (Hz)

h = diameter of the wire (cm)

L_m = mean length per turn (cm)

A_w =area of the wire (cm^2).

$\rho = 1.762*10^{-6}$ (Ω-cm)

2.6 Results of Power Losses Analysis

The selection of MOSFET has a major role in power losses analysis. The silicon carbide MOSFET has been considered for this case. As discussed earlier, high channel resistance affects the conduction losses. From Table 3, it can be found that SiC MOSFETs have lower high channel resistance, lower rise time and fall time (which reduces switching losses in MOSFETs) and superior thermal properties.

Table 3: SiC and Si MOSFET parameters

Parameters	CREE C2M028120D	Fairchild FQA8N100C
t_{fall}	21.7 ns	202 nS
t_{rise}	12.8 ns	145 ns
V_F	3.3 V	1.4 V
$R_{DS(ON)}$	280m Ω	1.45 Ω

Table 4 – Table 7 show the power losses and efficiency of the MOSFET CREE C2M028120D and the Fairchild FQA8N100C at 20kHz, 50kHz, and 100kHz in both Buck and Boost mode of BoCBB. In order to find the losses of the components in the circuit, several variables must be considered. In Buck mode, the Boost switch will be in the OFF state which leads to zero switching or conduction losses (Fig 5).

When it comes to Boost mode, the Buck switch will be in the ON state. Therefore, no switching losses are considered for S_{Buck}, but there will be conduction losses since it is in ON state.

With the frequency changes, the value of the inductor also changes, therefore, the number of turns (N) for the inductor changes. Since the conduction losses of diode and MOSFET are independent of frequency, they will be similar for different frequencies. For this circuit, the Schottky diode has been used. Only conduction losses are considered since switching losses for the Schottky diode are negligible. The core losses of the inductor are not significant for the diode and MOSFET, since the ΔB is small. Moreover, copper losses and core losses of the inductor depends on the type of core used.

Table 4: Losses of Fairchild MOSFET Buck mode (FQA8N100C)

Frequency		20kHz	50kHz	100kHz
		Buck mode	Buck mode	Buck mode
Core losses		$2.75*10^{-4}$W	$0.5*10^{-4}$W	$5.3*10^{-4}$W
Copper losses		0.6W	1.3W	1.32W
Switching losses		13W	32.5W	65W
Conduction losses	Buck side	65.25W	65.25W	65.25W
Diode losses		0.45W	0.45W	0.45W
Total Losses		79.3W	99.5	132.02W
Efficiency		97.35%	96.68%	95.59%

Table 5: Losses of Fairchild MOSFET Boost mode (FQA8N100C)

Frequency		20kHz	50kHz	100kHz
		Boost mode	Boost mode	Boost mode
Core losses		$1.15*10^{-4}$W	$0.55*10^{-4}$W	$1.6*10^{-3}$W
Copper losses		1.3W	1.3W	1.32W
Switching losses		7.5W	19.5W	39W
Conduction losses	Buck side	20.5W	20.5W	20.5W
	Boost side	61.2W	61.2W	61.2W
Diode losses		1.7W	1.7W	1.7W
Total Losses		92.2W	104.2	123.7W
Efficiency		96.92%	96.52%	95.87%

Table 6: Losses of SiC MOSFET Buck mode (C2M0280120D)

Frequency		20kHz	50kHz	100kHz
		Buck mode	Buck mode	Buck mode
Core losses		$2.75*10^{-4}$W	$0.5*10^{-4}$W	$5.3*10^{-4}$W
Copper losses		0.6W	1.3W	1.32W
Switching losses		1.25W	3.15W	6.3W
Conduction losses	Buck side	12.6W	12.6W	12.6W
Diode losses		0.45W	0.45W	0.45W
Total losses		15.35W	17.5W	20.03W
Efficiency		99.45%	99.4%	99.33%

Table 7: Losses of SiC MOSFET Boost mode (C2M0280120D)

Frequency		20kHz	50kHz	100kHz
		Boost mode	Boost mode	Boost mode
Core losses		$1.15*10^{-4}$W	$0.55*10^{-4}$W	$1.6*10^{-3}$W
Copper losses		1.3W	1.3W	1.32W
Switching losses		0.75W	1.9W	3.75W
Conduction losses	Buck side	3.95W	3.95W	3.95W
	Boost side	11.8W	11.8W	11.8W
Diode losses		1.7W	1.7W	1.7W
Total losses		19.4W	20.75W	22.52W
Efficiency		99.35%	99.31%	98.25%

CHAPTER 3
SLIDING WINDOW-COMBINED HYSTERSIS CONTROL TECHNIQUE

3.1 Introduction

A DC-DC power converter should generate a regulated DC output voltage under varying load and input voltage conditions. With the changing time, temperature, irradiance, pressure, the power converter component values also varies. Therefore, the control of the output voltage must be performed in a closed-loop manner using principles of negative feedback. Previously, several control methods have been applied in DC-DC power converters to meet specified requirements in control target. For example, the voltage control mode, current/power control mode, PID, and fuzzy logic controller [21]-[24].

3.2 Types of Control Methods

3.2.1 Voltage-mode control

Voltage mode control is the basic control mode shown in Fig 8 and consists of a single loop controller connected to a reference voltage. The first output voltage is measured by subtracting from the external reference voltage in an error amplifier. The error amplifier generates a control voltage compared to a constant amplitude sawtooth waveform. The PWM signal, generated by a comparator is fed to drivers of controllable switches in the DC-DC power converter. The value of the control voltages defines the duty ratio of the PWM signal. The frequency of the PWM signal is the same as the frequency of the sawtooth waveform [25]. The main advantage of the voltage-mode control is its simple hardware implementation based on the use of a feedback loop consisting solely of voltages and flexibility, i.e. the ability to control shorter on-time and high noise tolerance.

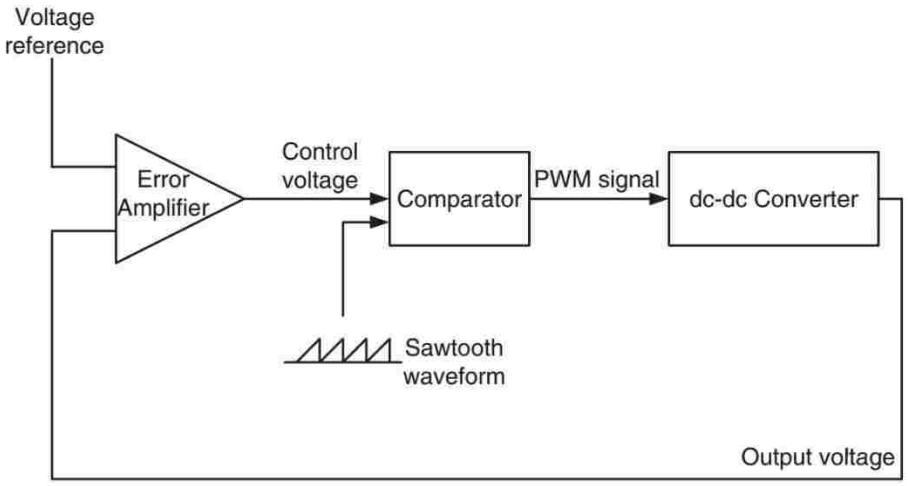

Fig 8. Voltage-mode control

The error amplifier responds quickly to the changes in the power converter output voltage. Therefore, the voltage-mode control provides good load regulation. However, line regulation, i.e. variation in the input voltage is delayed, changes in input must adjust themselves in the power converter output before they can be connected [25]. To solve this issue, the voltage-mode control scheme improves by a voltage feed forward path. The feed forward path directly affects the PWM duty ratio according to changes in the input voltage [25].

3.2.2 Current-mode control

Current-mode control shown in Fig 9 is the modified version of voltage-control mode. The sawtooth waveform in voltage-mode control is replayed by inductor current. The current sensing can be performed by using the on-resistance of the ongoing inductor current. This inductor current is passed to a comparator and can also be converted to analog voltage and compared to the control voltage. This replacement of the sawtooth waveform of the voltage-mode control scheme by a power converter signal extensively alters the dynamic behavior of the power converter [25]. The power converter depends on the characteristics of the current source. The output current in PWM DC-DC power converter is either equal to the average inductor current or a function of the duty ratio.

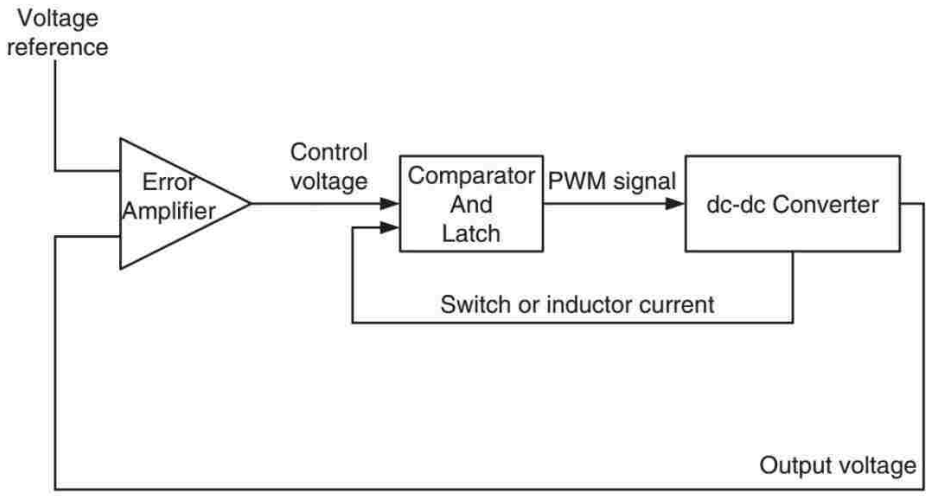

Fig 9. Current-mode control

In practical use, current-mode control senses the peak inductor current instead of the average current, since the peak current is equal to peak switching current [25]. Moreover, the peak inductor current is proportional to the input voltage. Therefore, the inner loop of the current-mode control inherently executes the input voltage feed forward technique. Since the current mode control has two types of feedback loops: voltage loop and current loop, the control implemented is relatively complex. Advantages of current-mode control include: input voltage feed forward, limit on the peak switch current, equal current sharing in modular power converters, and reduction in the power converter dynamic order. Along with the complexity, the low-noise tolerance due to the high sensitivity of current detection is also considered a major drawback for the current-mode control [25].

3.2.3 PID Controller

Proportional Integral and Derivational (PID) control, shown in Fig 10, is one of the old control techniques implemented on DC-DC power converters [26] [27]. It is operated on one of the control techniques which include proportional (P), proportional and derivational (PD), proportional and integral (PI), and proportional-integral and derivational (PID) controllers. These different controllers regulate DC power supply in various ways. PID is widely used for industrial applications in the field of power electronics. Easy implementation is one of the major reason for the use of PID techniques in industrial applications.

A PID controller uses feedback control mechanism, which is widely used in the research field. This control method is often considered as simple, reliable, and easy to implement.

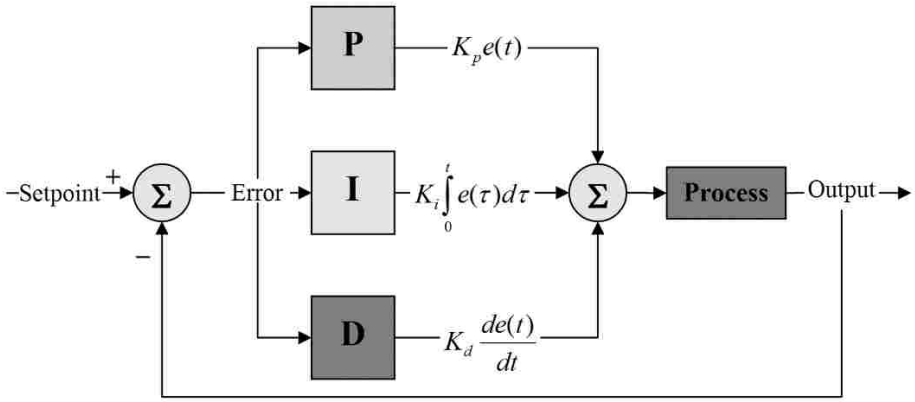

Fig 10. PID controller

PID controllers are easy and simple to implement and have a high reliability in linear systems. Disadvantages of PID controllers include being non-reliable in the case of non-linear systems, the fact that it has longer rise time when overshoot in output voltage deceases, and it suffers from dynamic response.

3.2.4 Fuzzy logic controller

Fuzzy logic, shown in Fig 11, solves some of the problems associated with PID controllers. It is non-linear, adaptive, and it is a practical alternative for a variety control applications [28]-[30]. The concept of Fuzzy logic (FL) was developed by Lotfi Zadeh, a professor from the University of California at Berkley. He states FL is not only a controller. It also processes data by allowing partial set membership functions rather than crisp ones. There are four main blocks in the fuzzy logic controller system structure: fuzzifier, rule base, inference engine and defuzzyfier. The working of the fuzzy logic controller can be explained in three steps: i. fuzzification, ii. inference and iii. defuzzification.

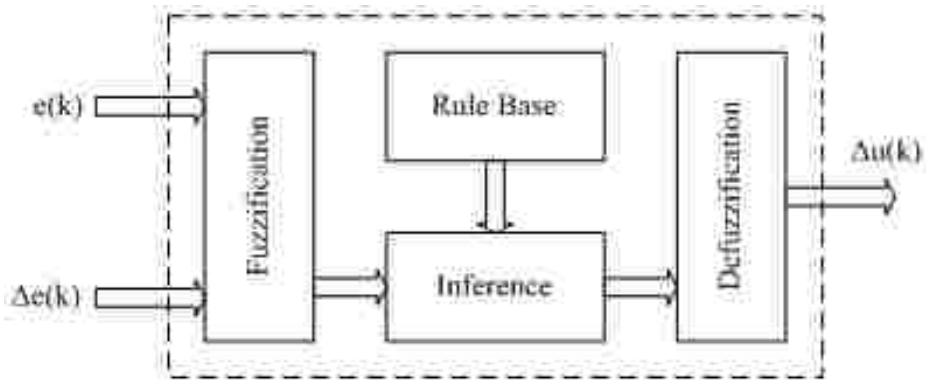

Fig 11. Fuzzy logic controller

The first step in the processes is the crisp set. It is used as input data, or non-fuzzy data, then it acts like a power converter to a fuzzy set using fuzzyfier with the help of linguistic variables, fuzzy linguistic terms, and membership functions. The important consideration in fuzzy logic is that a numerical value does not have to be fuzzified using only one membership function. Membership function is a curve that describes each point in the input space which is mapped to a membership value. Membership functions include Triangular, Gaussian, Trapezoidal, Generalized Bell, and Sigmoidal. Rule base is the backbone of fuzzy logic controllers. Steps performed by Rule Base block: i. The purpose of rule base is to control the output variable. ii. A fuzzy rule is a simple IF-THEN rule with a specific condition and conclusion, represented by the matrix table. iii. Error and change in error are the two variables taken along the axes, and the conclusions are within the table.

Advantages of fuzzy logic controllers are low-cost implementation based on low price sensors, low-resolution analog-to-digital power converters, fuzzy logic can be easily developed by adding new rules to improve performance or new features, it can be used for the improvement of traditional controller systems, it provides better performance under parameter variation and load disturbances, it operates at wide range conditions compared to PID, it can be operated with noise and disturbance of different natures and developing the fuzzy logic controller is much easier than developing a model based or other controller for the same work.

3.3 Transient Response

When the voltage from a solar panel is considered as input to the DC-DC power converters, the input voltage varies randomly and unpredictably within a certain range. These traditional control methods respond to transients and thus make DC-DC power converters transitioning from Buck mode to Boost mode or vice-versa. The transient response occurs whenever a sudden disturbance happens in a system. This transient response may cause voltage fluctuation in the output voltage and thus leads to instability in the system. The objective of the transient stability is to retain a steady output. Often change in modes leads to various transient responses for the output. Therefore, in this chapter, a novel sliding-window-combined (SWC) hysteresis control is designed to reduce the frequency of mode transition and improve voltage stability in the circumstances of quickly varying solar power.

In this chapter, the principle of the proposed SWC hysteresis control is introduced in Section 3.4, and its advantages over traditional hysteresis control are discussed and validated in Sections 3.4 and 3.5, respectively. Fig 12 indicates frequent mode transitions when there is fluctuation around the threshold of 400 volts. The solar power data are sampled from a real application [web]. In Fig. 12 and other plots, orange lines indicate the operation mode (i.e. Buck or Boost mode) of the BoCBB power converter. The voltage level of 402 volts indicates the Buck mode and the 398 volts indicates the Boost mode in the BoCBB power converter.

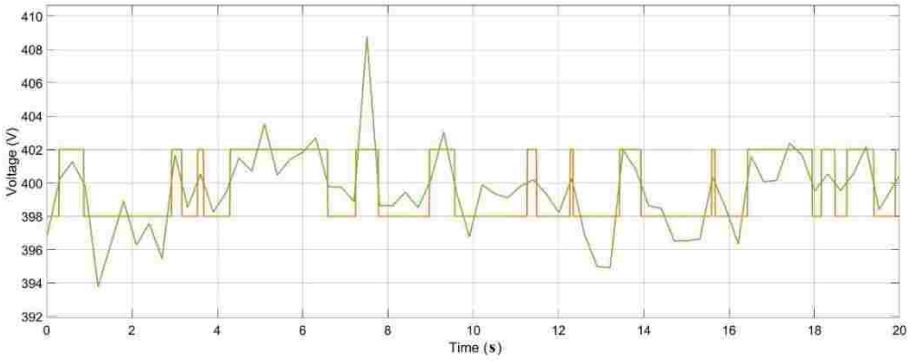

Fig 12. Mode selection of BoCBB for varying input

At first, the hysteresis controller for mode transition is introduced. The drawback of traditional hysteresis controllers in voltage stability is discussed. Based on that, the principle of a SWC hysteresis controller is developed by integrating a sliding window into the hysteresis controller to control the number of mode transitions freely.

3.3 Hysteresis Controller

Considering the rated input voltage of 400 volts, the hysteresis control is expected to reduce the number of mode transitions, when the input solar voltage varies around the 400 volts. The hysteresis controller is designed with threshold voltages for the two modes as shown in Fig. 13 The BoCBB solar power converter transits from Boost mode to Buck mode when the solar input voltage exceeds the upper boundary of 402 volts (assuming input voltage varies from 390 volts to 410 volts). And the BoCBB power converter transits from Buck mode to Boost mode when the solar input voltage reaches below the lower boundary of 398 volts.

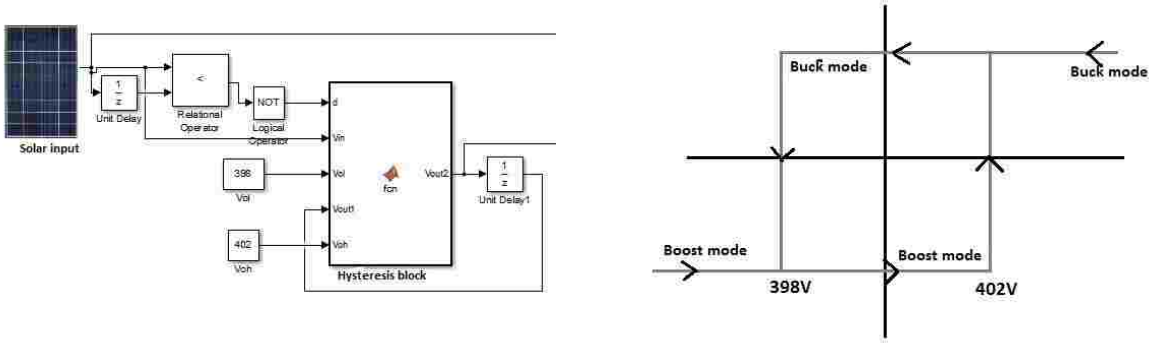

Fig 13. Hysteresis control blocks in Matlab simulation and defined boundary values of a traditional hysteresis controller

In Fig 14, the term of Vin(t)-Vin(t-1) is used to evaluate the increase or decrease of input solar voltage in amplitude by comparing initial input with the input value of previous time step over a unit delay. V_{OH} is the upper threshold voltage and V_{OL} is the lower threshold voltage. V_{OUT} (t-1) defines the mode of

previous time interval of the hysteresis control. V_{OUT}(t-1) is used to avoid mode transition when the input voltage oscillates within the defined range of threshold voltages.

The flow chart shown in Fig 14 explains that if the term of Vin(t)-Vin(t-1) is greater than or equal to one, the solar input voltage is increasing and the controller should transit into Buck mode only when the input goes over upper threshold voltage (*i.e.* 402 volts in this study). Otherwise, the controller remains staying in Boost mode. Similarly, when the term of Vin(t)-Vin(t-1) less than or equal to one, the controller should transit into Boost mode only when the input goes below lower threshold value (i.e. 398 volts in this study). Otherwise, the controller remains operating in Buck mode.

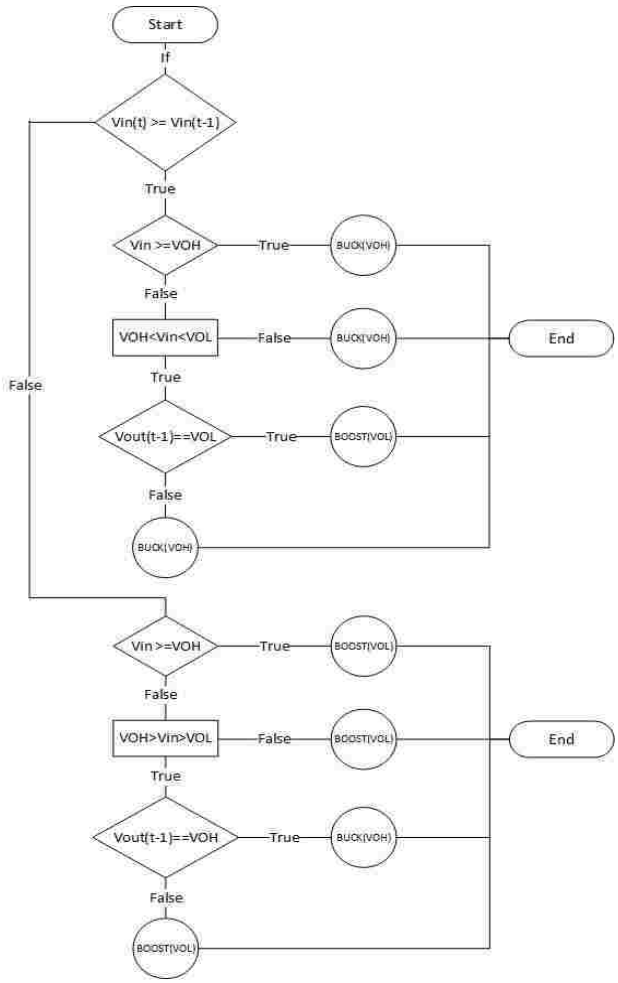

Fig 14. Flow chart to control the mode transition based on the concept of traditional hysteresis loop.

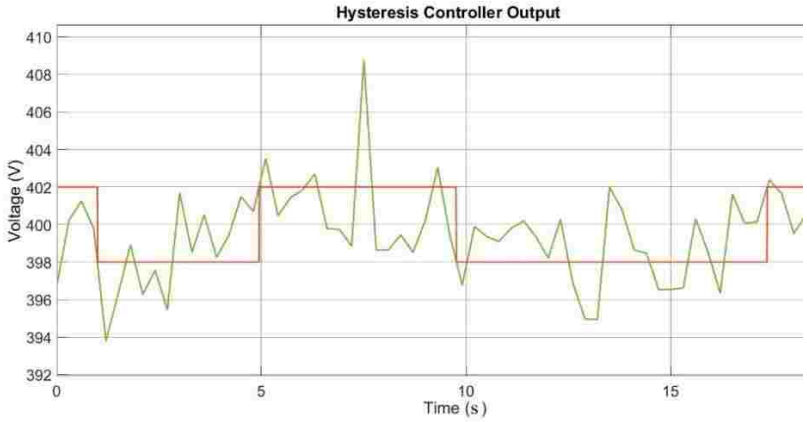

Fig 15. Mode transition of BoCBB power converter under specified traditional hysteresis control

Comparing Fig. 13 and Fig. 15, it is noted that the number of mode transitions can be greatly reduced by applying traditional hysteresis control. In this case, the number of mode transitions reduces from 21 to 4 in the data period. But there are some considerations of importance, which lead to the disadvantage of using traditional hysteresis control in this application. There is a limitation in the duty cycle of BoCBB solar power converters. Assuming the BoCBB power converter is in Boost mode initially, the power converter remains in Boost mode unless the input solar voltage exceeds the upper threshold voltage. But when the input solar voltage is within (400V- 402V) and the power converter is in Boost mode, the duty cycle for Boost mode will be:

$$D_{Boost} = 1 - \frac{Vin}{Vout} \tag{27}$$

$$(e.g.\ D_{Boost} = 1 - \frac{402}{400} = -0.005)$$

Obviously, a negative duty cycle is theoretically impossible and the duty cycle has to be restricted to ‘0’. Under this condition, there is an overvoltage reflected in the output voltage until the input solar voltage exceeds the upper threshold and the mode transits into Buck mode. Similarly, the duty cycle of the Buck mode cannot go over ‘1’ theoretically and has to be limited to ‘1’. Within this stand-by mode transition status, there is a voltage sag reflected in the output voltage.

$$D = \frac{Vout}{Vin} \tag{28}$$

(*e.g.* $D = \frac{400}{398} = 1.005$)

Overall, the traditional hysteresis control results in overvoltage and voltage sag during transients of mode transitions in the application of DC-DC solar conversion. This problem can be fixed by integrating sliding-window into the hysteresis controller. A larger width of the hysteresis loop leads to a smaller number of mode transitions but a larger voltage fluctuation.

3.5 Sliding Window-Combined Hysteresis Controller

The weakness in traditional hysteresis control can be compensated by using a sliding window to the input of hysteresis control to form a sliding-window-combined hysteresis control – the SWC hysteresis control. The block diagram of SWC hysteresis controller is shown in Fig 16. The width of the sliding window (the integration time) is kept as a pre-selected constant to calculate the mean value of the input solar voltage over a period of time:

$$\text{Mean of f(t)} = \frac{1}{T}\int_{t-T}^{t} f(t).dt \tag{29}$$

where T = the width of sliding window in seconds

f = 1/T.

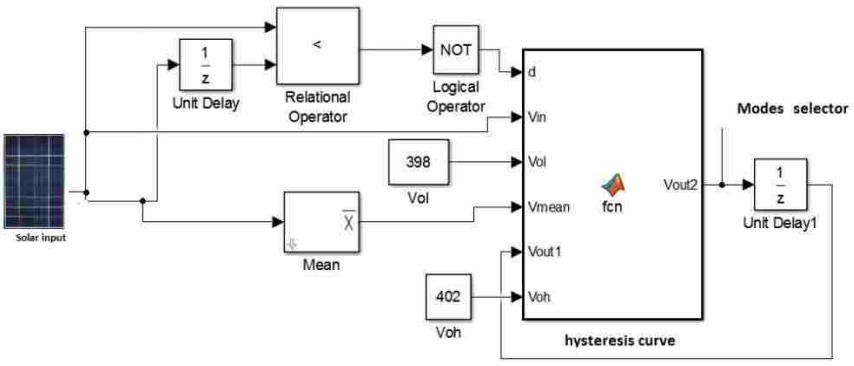

Fig 16. Control block of sliding-window-combined hysteresis control

Based on the baseline BoCBB power converter, a series of tests were performed by changing the window width T in the SWC hysteresis control. Comparing to Fig 17 (a), Fig 17(e) shows that the number of mode transition is directly dependent on the width of sliding window.

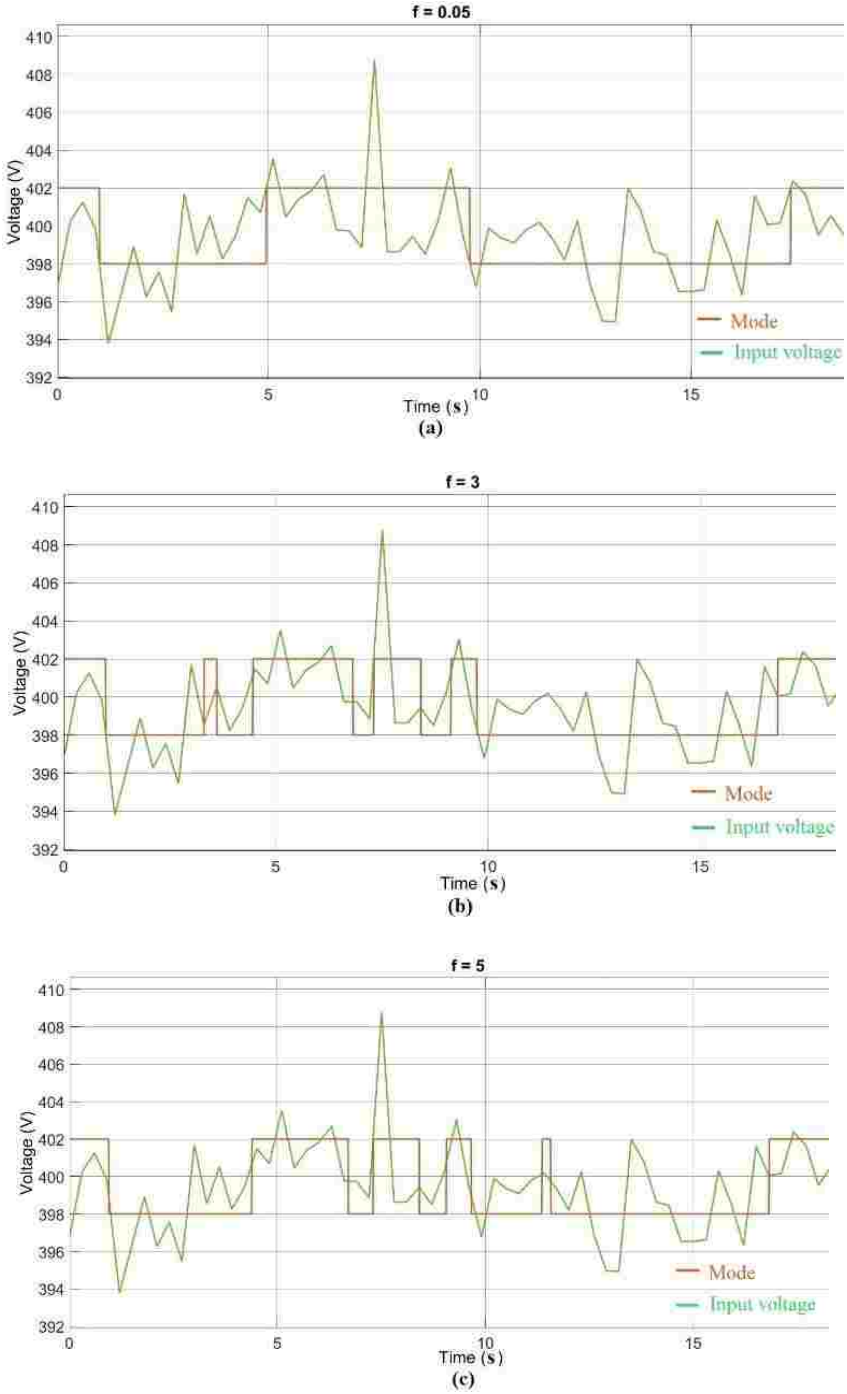

Fig 17. Comparing the number of mode transition
under different width in sliding window

Fig 17. (Cont.)

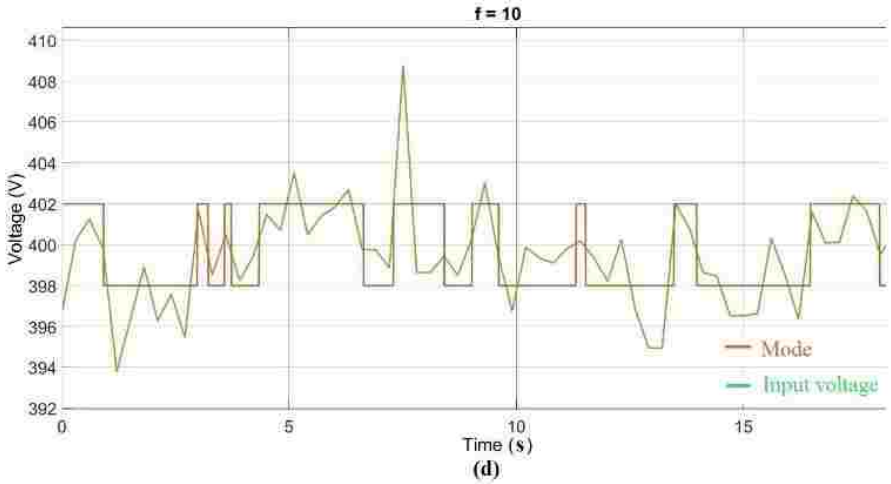

(d)

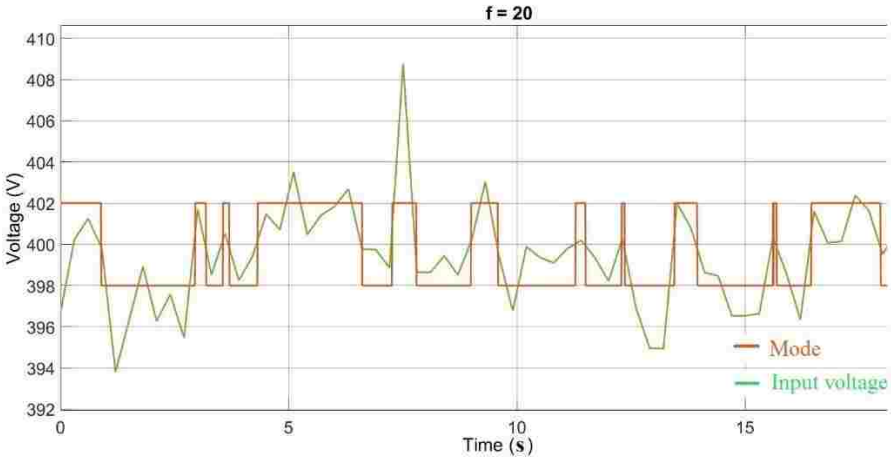

(e)

With the decrease in frequency, the sliding window width increases and vice-versa. With a low frequency, the mean of the input is considered across higher time lengths, which leads to decrease in change of mode. From Fig 17 (a) it can be concluded as the sliding window concept behavir is similar to the hystersis controller at lower frequencies. With high frequency, the mean of the input is considered across the lower time lengths which leads to an increase in the change of mode. From Fig 17 (e) it can be concluded that the sliding window concept behaviour is similar to the voltage mode controller. The minimal frequency can be considered in order to adjust the change in modes for given input time length.

CHAPTER 4

SIMULATION & PCB DESIGN OF BoCBB POWER CONVERTER

4.1 Simulation Block of BoCBB Power Converter

A simulation was performed by using Simulink software. Fig 18 shows the Simulink block diagram of BoCBB DC-DC power converter. The Proportional and Integral (PI) controller is used to eliminate steady state error resulting from the P controller. A low pass filter is connected as the input for the feedback loop to block the high frequency voltage and allow the low frequency output voltage. As discussed in Chapter 3, error voltage can be found by comparing the output voltage with the reference voltage. This error voltage is given to the PI controller, which generates voltage to adjust the duty cycle of the both swtiches. The PWM generator is used to generate pulses, the width of the pulses are adjusted by using duty cycle.

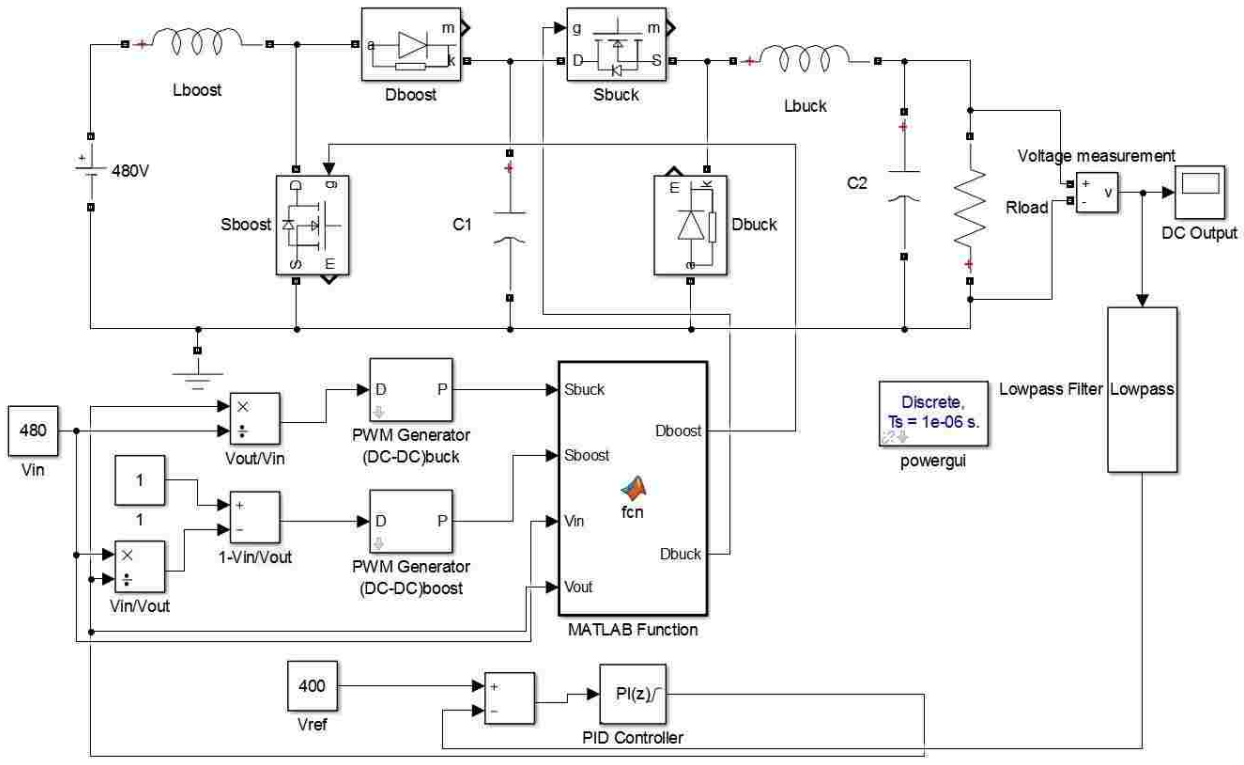

Fig 18. Simulink model of Boost-cascaded Buck-Boost power converter

The component values considered for BoCBB DC-DC power converter are shown in Table 8.

Table 8: Component values of Simulink BoCBB circuit

	Buck mode	Boost mode
V_{in}	480V	300V
L1	5.6 mH	5.6 mH
L2	4.4 mH	4.4 mH
C1	100 nF	100 nF
C2	50 µF	50 µF
R_{load}	53.3 Ω	53.3 Ω
V_{out}	400V	400V

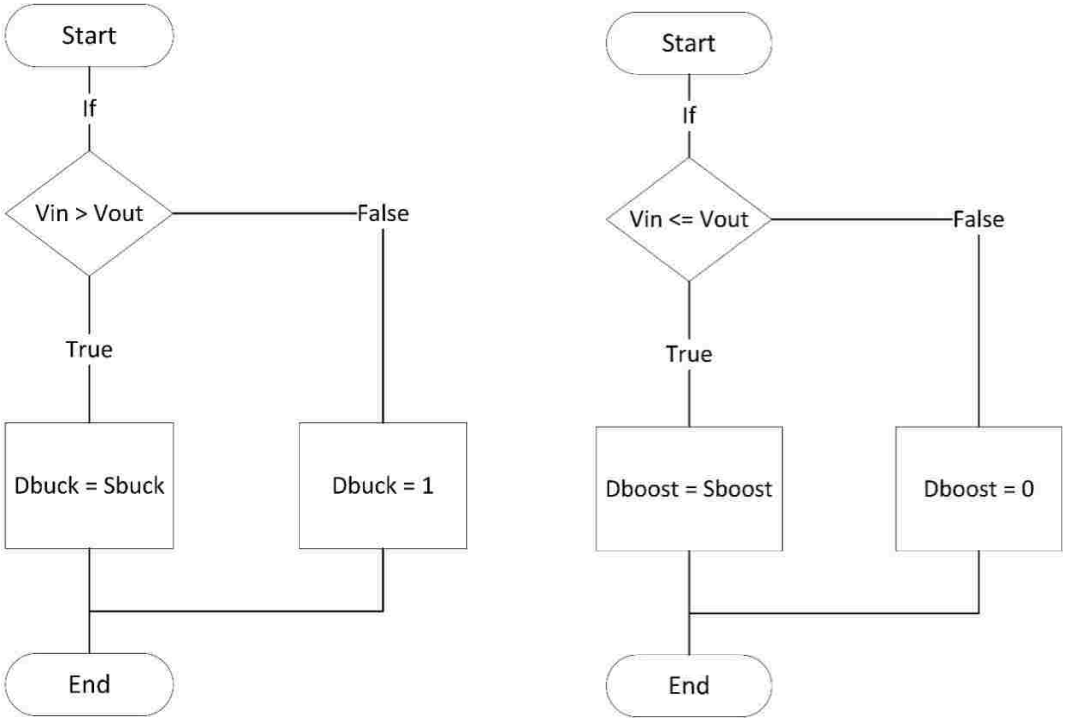

Fig 19. Flowchart for the selection of switches based on input and output voltages

The Matlab function consists of the logical program shown in Fig 19. This flow chart explains the selction of pulse signal to the switching operation at the Boost side (D_{Buck}) and the Buck-Boost side (D_{Boost}). When the input voltage is greater than the output voltage, D_{Buck} is equal to the pulse signal with a duty cycle of $\frac{V_{out}}{V_{in}}$ gernerated from PWM generater (Buck) and D_{Boost} equals to zero since the Boost switch will be in off state which does not allow current to pass to the ground. When the input voltage is less than or equal to the output voltage, D_{Buck} is equal to one (D_{Buck} should be always on in order to pass the current to the load side) and D_{Boost} equals the pulse signal with a duty cycle of $1 - \frac{V_{in}}{V_{out}}$ generated from the PWM generator (Boost). Fig 20- Fig 23 shows the simulation results of Boost-Cascaded Buck-Boost power converter (BoCBB) in Buck mode.

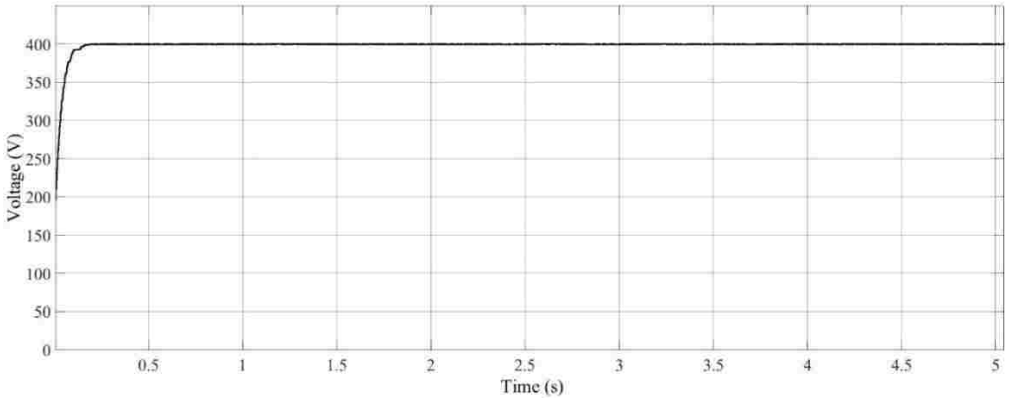

Fig 20. BoCBB output in Buck mode

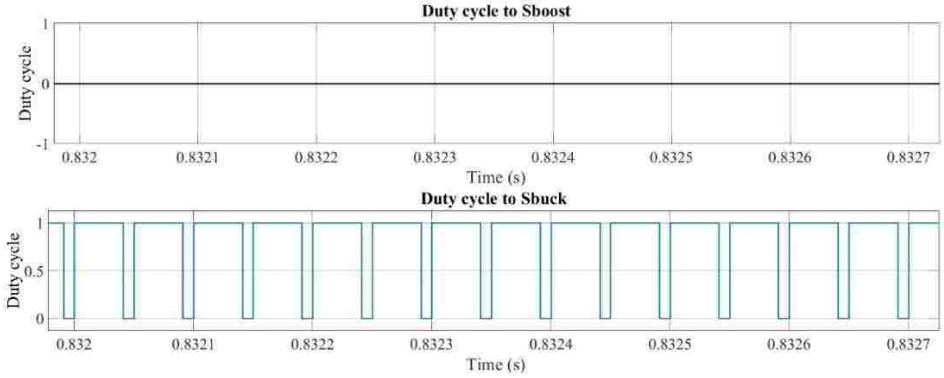

Fig 21. Duty cycle of S_{Boost} and S_{Buck} of BoCBB in Buck mode

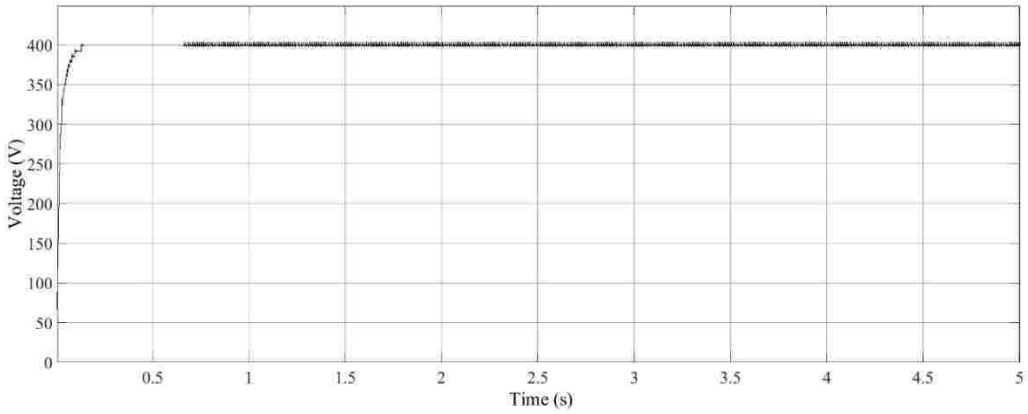

Fig 22. BoCBB output in Boost mode

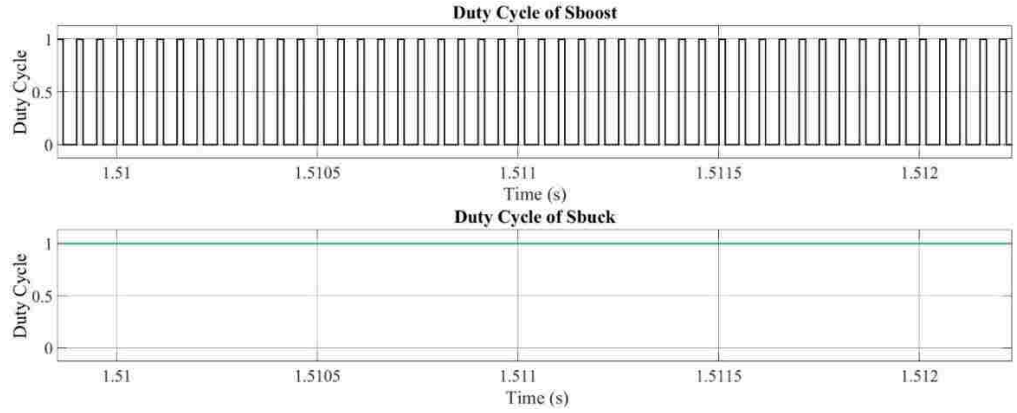

Fig 23. Duty cycle of S_{Boost} and S_{Buck} of BoCBB in Boost mode

4.2 Driver Circuit of SiC MOSFET

The key features of the SiC MOSFET are: low R_{DS}(on) and small R_{DS}(on) change over operating temperature range; fast switching transient times, low capacitances; easy to parallel, and easy to drive. The SiC MOSFET is positioned to replace silicon MOSFETs and IGBTs in high efficiency, high switching frequency power conversion applications. In order to drive the CREE MOSFET for the Boost cascaded Buck-Boost (BoCBB) power converter, the isolated driver circuit is used.

The isolated driver circuit, shown in Fig 24, consists of two DC-DC power converters, an Opto-Isolator (HCPL 3180) and the gate driver (IXYS IXD 609). The function of the DC-DC power converters

is to generate $+V_{EE}$ and $-V_{CC}$ to the Opto-Isolator and to the gate driver. The gate driver can generate an output voltage 35V and + or _ 9A current. The function of Opto-Isolator is to generate output ranging from 0 to 20V, which is used as input for the gate driver.

As already mentioned DC-DC power converters DC1 (RP 1212D) and DC2 (RP 1205S) are used to generate $+V_{CC}$ as 12V and $-V_{EE}$ as 5V, to make sure V_{CC} -V_{EE} is less than 20V. In case V_{CC} -V_{EE} goes over 20V, to limit the voltage to 19V for V_{CC} of the Opto-Isolator (Since $V_{CC} - V_{EE}$ range for IC 1 (HCPL) is 10V to 20V) the emitter-follower circuit consisting of Transistor T1 and Diode D1 is used. A resistor R16 is included for additional damping. A variable resistor has been used to control the control the voltage. Table 9 shows the component values of the driver circuit for BoCBB power converter.

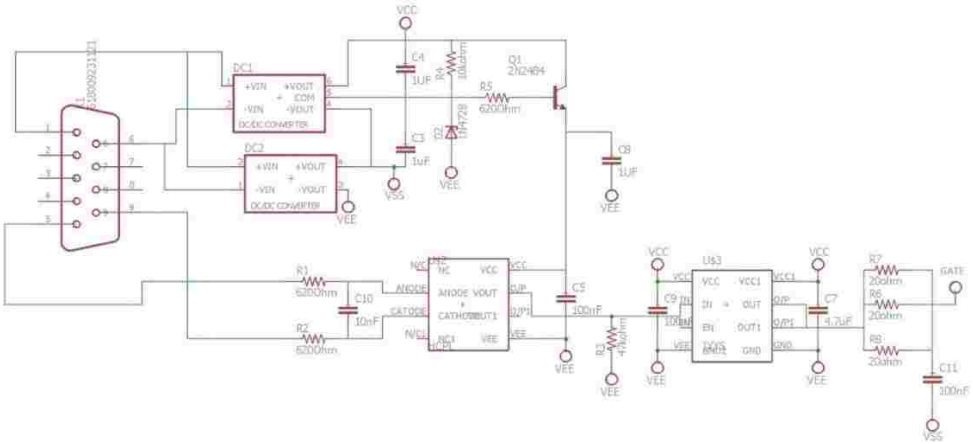

Fig 24. Circuit Diagram of CREE SiC MOSFET driver

Table 9: Component values of SiC driver circuit

Components	**Values**
Capacitor (C3, C4, C8)	1µF
Capacitor (C5, C9, C11, C12)	100nF
Capacitor (C6, C7	4.7µF

C10)	10nF
Resistor (R1, R2, R5)	620 Ω
Resistor (R3)	47k Ω
Resistor (R4)	100k Ω
Resistor (R6, R7, R8, R9, R10, R11)	20 Ω
DC-DC power converter (DC1)	RP1212D (12V-12V)
DC-DC power converter (DC2)	RP1205S (12V-5V)
Opto-Isolator	(HCPL 3180)
Gate driver	IXYS IXD 609

4.3 Printed Circuit Board (PCB) design of BoCBB Power Converter

Schematic diagram of BoCBB PCB board is shown in Fig 25. Several things have been considered while designing the PCB board shown in Fig 26.

a) The components of high power side shown in Fig 27 share a different top layer and the components of the control circuit (low power side) share another top layer. This separation avoids the contact of heat dissipation at the high power circuit with the lower power circuit, but the both high power elements and control circuit elements share a common ground, as shown in Fig 28.

b) The heat sinks are connected to the MOSFETs and Schottky diodes to release the heat generated due to the power loss at the MOSFETs and Schottky diodes. The back side of MOSFETs and Schottky diodes, which release heat, are faced outwards of the PCB board.

c) The width of the connection lines of high power circuit is thicker than lower power circuit (control circuit).

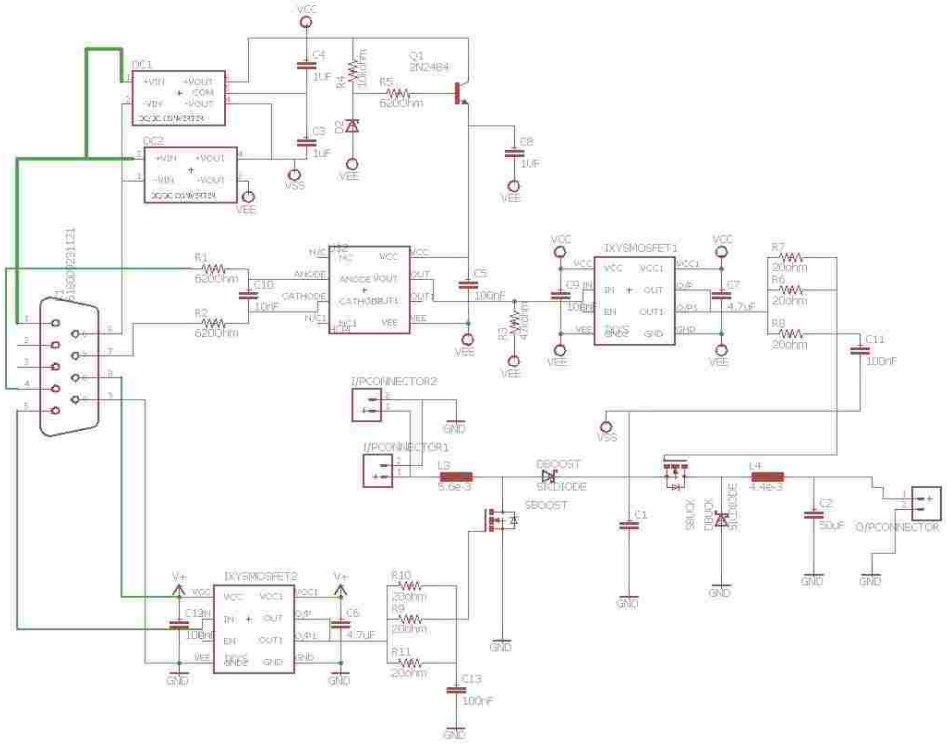

Fig 25. PCB Schematic diagram of BoCBB with driver circuit

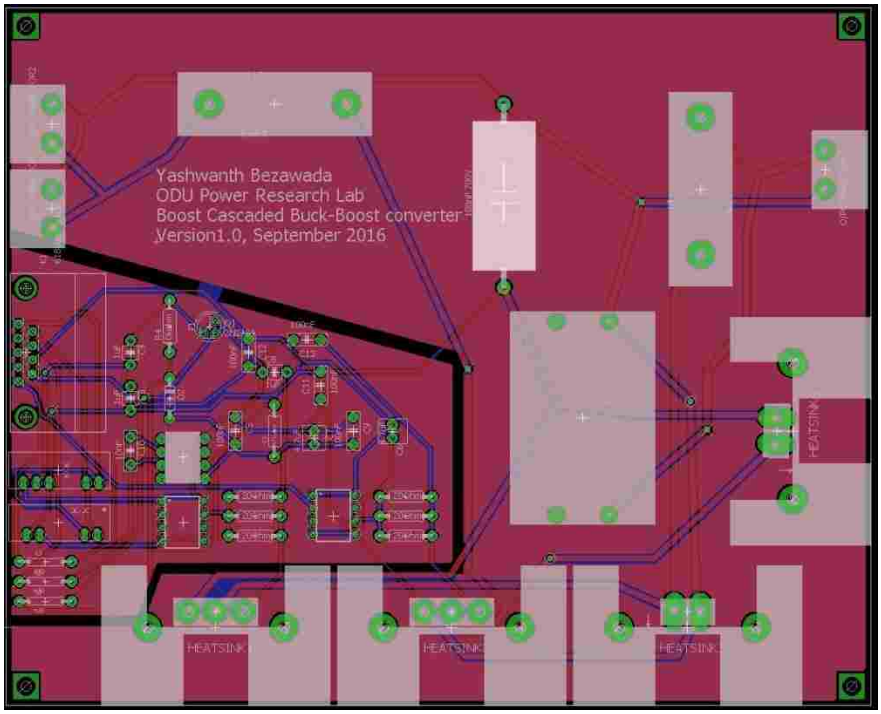

Fig 26. PCB board of BoCBB with driver circuit

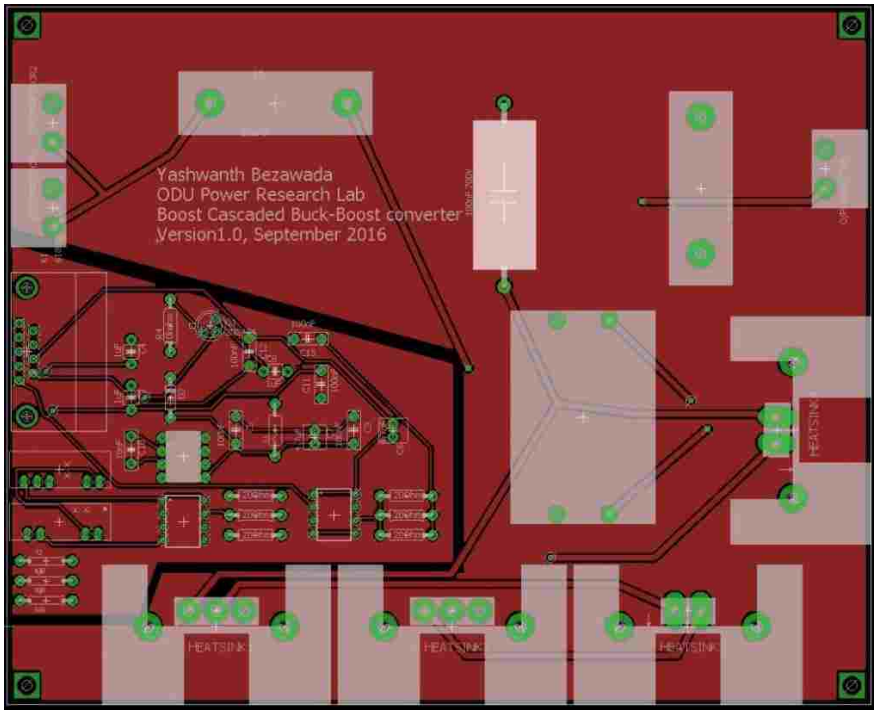

Fig 27. Top layer of the BoCBB PCB board

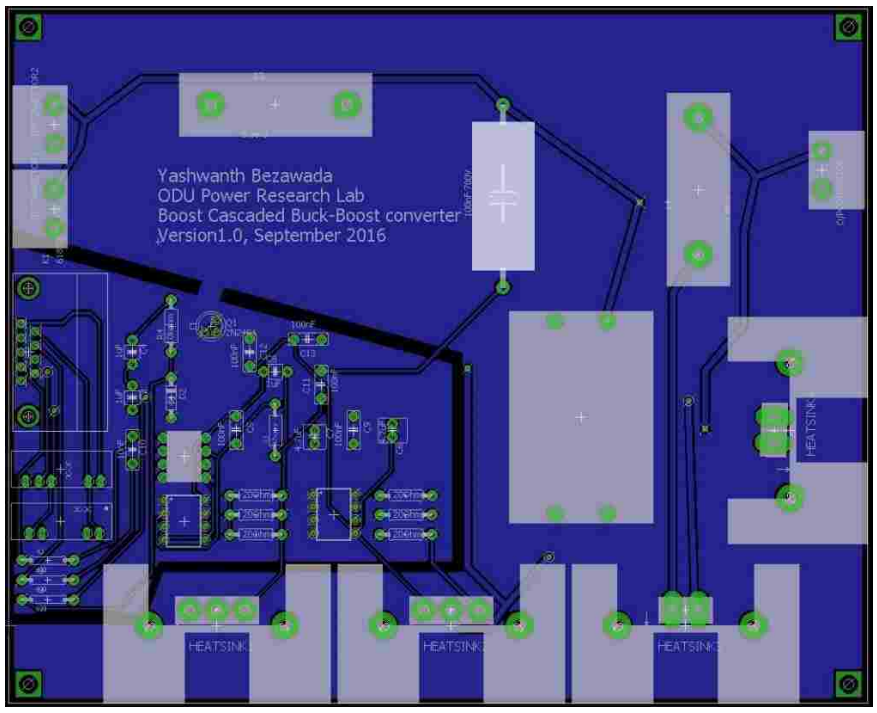

Fig 28. Ground layer of the BoCBB PCB board

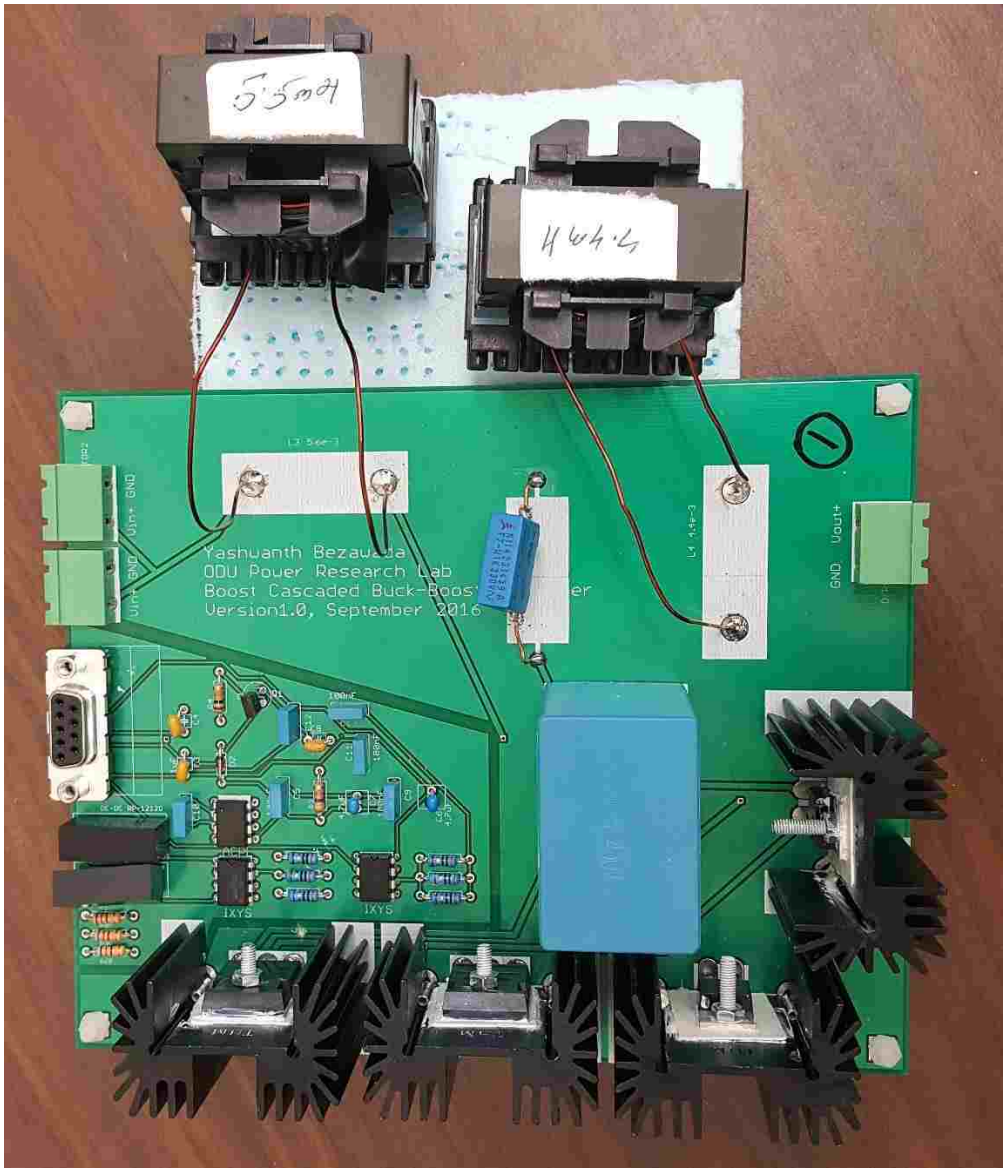

Fig 29. PCB Board of BoCBB

As shown in Fig 29, a Silicon carbide compound is applied to achieve proper insulation between the heat sink and MOSFETs as well as the Schottky diodes. It protects the MOSFETs and Schottky diodes by connecting the components firmly to the heat sink, which results in release of heat quickly and equally.

CHAPTER 5

EXPERIMENTAL RESULTS

A hardware test is performed by using BoCBB PCB board for 200W power by using two 100Ω loads in series shown in Fig 31. Fig 30 represents the schematic diagram of experiment conducted on BoCBB in Boost mode. The experimental results are represented in Table 10 to Table 12. Since the input current is proportional to the duty cycle of the Boost power converter, for the higher duty cycle at the Boost inductor, the L1 current flow is high. High current leads to more power losses at MOSFET, inductor, and Schottky diode. Hence, for high duty cycles, power losses are high. Tables 10 to Table 12 proves the statement by comparing efficiency of Boost power converters for duty cycle 0.5 and 0.1 at 20kHz, 50kHz, and 100kHz frequency. The efficiency decreases from 3-5% from 20kHz to 100kHz for different duty cycles. As mentioned in Chapter 3, the below results prove that with the increase in frequency, the power losses also increase since switching losses of MOSFET and copper losses of the inductor depends on the switching frequency of the DC-DC power converter. The efficiency decreases from 3-5% from 20kHz to 100kHz with the same duty cycle.

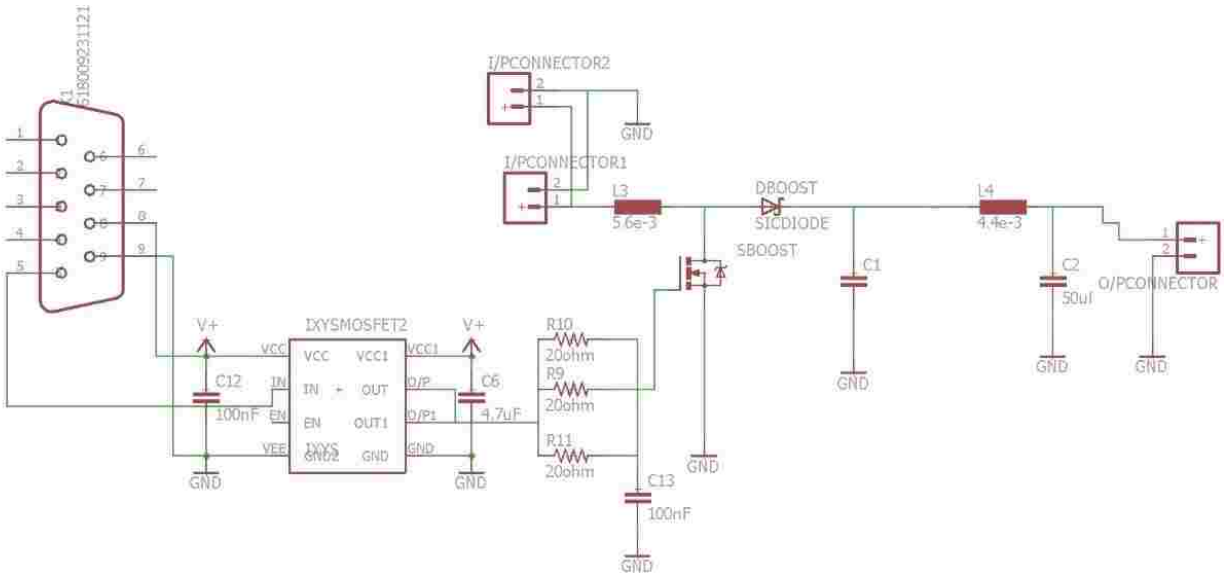

Fig 30. Circuit diagram of BoCBB in Boost mode

The performance of the inductor plays an important role for conducting the hardware test of BoCBB power converter in Boost mode. Since high current flows through the Boost inductor for high duty cycle the EE 40 core goes into saturation for high currents which affects the performance of the circuit. In order to avoid the saturation, the permeability of the inductor has been increased. The increase in permeability leads to increase in number of turns for EE40 core, which leads to increase in copper losses of inductor (since copper losses depends number of turns).

Fig 31. Hardware test of BoCBB in Boost mode

Table 10: Efficiency of BoCBB in Boost mode at frequency = 20 kHz of R_{load} = 200.8 Ω

D	**V_{in}**	**I_{in}**	**V_{out}**	**I_{out}**	**η % = P_{out}/P_{in}**
0.5	108.9V	1.94A	200.1V	0.996A	94.43%
0.4	126.5V	1.65A	200.1V	0.996A	95.48%
0.3	145.2V	1.42A	200.1V	0.996A	96.61%
0.2	164.2V	1.25A	200.2V	0.997A	97.24%
0.1	183.1V	1.11A	200.2V	0.997A	98.20%

Table 11: Efficiency of BoCBB in Boost mode at frequency = 50 kHz of R_{load} = 200.8 Ω

D	V_{in}	I_{in}	V_{out}	I_{out}	η % = P_{out}/P_{in}
0.5	106.5V	2.01A	200.4V	0.998A	93.42%
0.4	125.4V	1.68A	200.2V	0.997A	94.97%
0.3	144.3V	1.44A	200.2V	0.997A	96.05%
0.2	163.9V	1.26A	200.2V	0.997A	96.65%
0.1	183.9V	1.12A	200.2V	0.997A	97.01%

Table 12: Efficiency of BoCBB in Boost mode at frequency = 100 kHz of R_{load} = 200.8 Ω

D	V_{in}	I_{in}	V_{out}	I_{out}	η % = P_{out}/P_{in}
0.5	107.2V	2.08A	201.1V	1.0A	90.32%
0.4	125.6V	1.73A	200.8V	1.0A	92.41%
0.3	145.1V	1.47A	200.3V	0.997A	93.62%
0.2	165.1V	1.28A	200.2V	0.997A	94.42%
0.1	187.1V	1.12A	200.2V	0.997A	95.25%

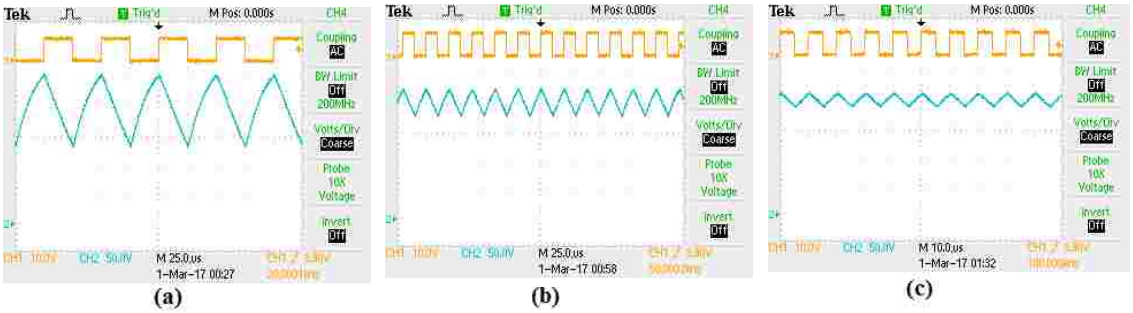

(a) (b) (c)

Fig 32. The waveform at capacitor C1 at (a) 20 kHz (b) 50 kHz and (c) 100 kHz

From Fig 32, the peak-peak voltage at capacitor increases with the decrease in frequency. An increase in peak-peak voltage leads to a higher current from capacitor to Buck inductor L2. This applies more stress on the inductor L2, which leads to saturation of EE 40 core. A heavy current chassis mount inductor shown in Fig 33, has been used to improve the performance of the LCL for BoCBB in Boost mode.

Fig 33. Heavy current chassis mount inductor

Even though, a heavy current chassis mount inductor improves the performance of the filter, it generates additional power losses compared to the EE 40 core. A Heavy current chassis mount inductor is applicable for low frequencies which leads to generation more power losses in high frequency circuits.

CHAPTER 6

CONCLUSION AND FUTURE WORK

6.1 Conclusion

Even though the efficiency of BoCBB is greater at 20kHz frequency (94.43%), the peak-peak voltage of capacitor C1 =125V is considered the concern of the performance of LCL filter. Since the peak-peak voltage of capacitor C1= 60V at 50kHz is lower than peak-peak voltage of capacitor C1 at 20kHz. LCL filter of BoCBB at 100kHz has the better performance since peak-peak voltage of capacitor C1=50V, but the efficiency of the BoCBB at 100kHz = 90.32% which is lower than the efficiency at 50kHz = 93.42%. From theoretical results found in Chapter 3, the power losses of BoCBB in Boost mode is greater than the BoCBB in Buck mode. Therefore, the efficiency measured in experimentation is the minimum for the BoCBB. This leads to the conclusion that 50kHz switching frequency is more suitable for performance of BoCBB DC-DC power converter and also BoCBB is highly efficiency at 50kHz.

6.2 Future Work

Future work will focus on performing experiments to analyze the sliding window concept in a hardware-in-the-loop (HIL) testbed. The sliding window method is expected to minimize the transients caused by frequent mode transition in the BoCBB power converter.

References

1. D.Feldman, D. Boff and R. Margolis. “Q2/Q3 2016 presentation – solar industry update”. Internet.https://energy.gov/eere/sunshot/q2q3-2016-presentation-solar-industry-update [Oct. 11, 2016].
2. H. Bellia, R. Youcef, and M. Fatima, "A detailed modeling of photovoltaic module using MATLAB," *NRIAG Journal of Astronomy and Geophysics,* vol. 3, pp. 53-61, 2014.
3. M. Seyedmahmoudian, S. Mekhilef, R. Rahmani, R. Yusof, and E. T. Renani, "Analytical modeling of partially shaded photovoltaic systems," *Energies,* vol. 6, pp. 128-144, 2013.
4. S. Surawdhaniwar and M. R. Diwan, "Study of Maximum Power Point Tracking Using Perturb and Observe Method," *International Journal of Advanced Research in Computer Engineering & Technology (IJARCET),* vol. 1, pp. pp: 106-110, 2012.
5. T. Esram and P. L. Chapman, "Comparison of photovoltaic array maximum power point tracking techniques," *IEEE Transactions on energy conversion,* vol. 22, pp. 439-449, 2007.
6. R. Faranda and S. Leva, "Energy comparison of MPPT techniques for PV Systems," *WSEAS transactions on power systems,* vol. 3, pp. 446-455, 2008.
7. R. Leyva, C. Alonso, I. Queinnec, A. Cid-Pastor, D. Lagrange, and L. Martinez-Salamero, "MPPT of photovoltaic systems using extremum-seeking control," *IEEE transactions on aerospace and electronic systems,* vol. 42, pp. 249-258, 2006.
8. C.-H. Chang, C.-A. Cheng, E.-C. Chang, and H.-L. Cheng, "Design and implementation of a two-switch Buck-Boost typed inverter with universal and high-efficiency features," in *Power Electronics and ECCE Asia (ICPE-ECCE Asia), 2015 9th International Conference on*, 2015, pp. 2737-2743.
9. Y. Yang, J. Ma, J. Ye, and Z. Han, "A new coupled inductors used in interleaving bidirectional DC/DC converter," in *Power Electronics and Application Conference and Exposition (PEAC), 2014 International*, 2014, pp. 1014-1019.

10. C.-M. Wang, C.-H. Lin, C.-C. Wu, and C.-W Chuang. “A Soft-Switching Interleaved Boost DC/DC Power converter”. Proc. *In Electrical machines and Systems (ICEMS)*, 016 19th International conference on November 13-16, 2016.

11. W. Li and X. He, "ZVT interleaved Boost converters for high-efficiency, high step-up DC-DC conversion," *IET Electric Power Applications*, vol. 1, pp. 284-290, 2007.

12. L. Guo, J. Y. Hung, and R. Nelms, "Comparative evaluation of linear PID and fuzzy control for a Boost converter," in *Industrial Electronics Society, 2005. IECON 2005. 31st Annual Conference of IEEE*, 2005, p. 6 pp.

13. S. Kapat and P. T. Krein, "Formulation of PID control for DC–DC converters based on capacitor current: A geometric context," *IEEE Transactions on Power Electronics*, vol. 27, pp. 1424-1432, 2012.

14. A. Sugiki and K. Furuta, "POSICAST control design for parameter-uncertain plants," in *Decision and Control, 2006 45th IEEE Conference on*, 2006, pp. 3192-3197.

15. B. S. Prasad, S. Jain, and V. Agarwal, "Universal single-stage grid-connected inverter," *IEEE Transactions on Energy Conversion*, vol. 23, pp. 128-137, 2008.

16. Y.-C. Chang, C.-L. Kuo, K.-H. sun, and T.-C. Li. “Development and operational control of two-string maximum power point trackers in DC distribution systems”. *IEEE Transactions. Power Electron.* vol. 28, no. 4, pp. 1852-1861, Apr. 2013.

17. C.-L. Wei, C.-H. Chen, K.-C. Wu, and I.-T. Ko, "Design of an average-current-mode noninverting Buck–Boost DC–DC converter with reduced switching and conduction losses," *IEEE Transactions on Power Electronics*, vol. 27, pp. 4934-4943, 2012.

18. J. Chen, D. Maksimovic, and R. W. Erickson, "Analysis and design of a low-stress Buck-Boost converter in universal-input PFC applications," *IEEE Transactions on Power Electronics*, vol. 21, pp. 320-329, 2006.

19. N. Mohan and T. M. Undeland, *Power electronics: converters, applications, and design*: John Wiley & Sons, 2007.
20. R. W. Erickson and D. Maksimovic, *Fundamentals of power electronics*: Springer Science & Business Media, 2007.
21. S. Saggini, P. Mattavelli, M. Ghioni, and M. Redaelli, "Mixed-signal voltage-mode control for DC–DC converters with inherent analog derivative action," *IEEE Transactions on Power Electronics*, vol. 23, pp. 1485-1493, 2008).
22. H. Peng and D. Maksimovic, "Digital current-mode controller for DC-DC converters," in *Applied Power Electronics Conference and Exposition, 2005. APEC 2005. Twentieth Annual IEEE*, 2005, pp. 899-905.
23. S. Kapat and P. T. Krein, "PID controller tuning in a DC-DC converter: A geometric approach for minimum transient recovery time," in *Control and Modeling for Power Electronics (COMPEL), 2010 IEEE 12th Workshop on*, 2010, pp. 1-6.
24. M. Shamim-Ul-Alam, M. Quamruzzaman, and K. Rahman, "Fuzzy logic based sliding mode controlled dc-dc Boost converter," in *Electrical and Computer Engineering (ICECE), 2010 International Conference on*, 2010, pp. 70-73.
25. M. H. Rashid, *Power electronics handbook: devices, circuits and applications*: Academic press, 2010.
26. S. Kapat. and P.T Krein. " PID controller tuning in a DC-DC power converter: A geometric approach for minimum transient recovery time", Proc. *in Control and Modeling for Power Electronics (COMPEL)*, 2010 IEEE 12th Workshop, pp. 1-6(2010).
27. Z. Wu, J. Zhao, and J. Zhang, "Cascade PID control of Buck-Boost-type DC/DC power converters," in *Intelligent Control and Automation, 2006. WCICA 2006. The Sixth World Congress on*, 2006, pp. 8467-8471.

28. I. Eker and Y. Torun, "Fuzzy logic control to be conventional method," *Energy conversion and management*, vol. 47, pp. 377-394, 2006.

29. P. Carbonell, G. Garcerá, and A. Hilario, "Fuzzy gain scheduling control of switch-mode dc/dc converters," in *Industrial Electronics, 1999. ISIE'99. Proceedings of the IEEE International Symposium on*, 1999, pp. 403-407.

30. M. Shamim-Ul-Alam, M. Quamruzzaman, and K. Rahman, "Fuzzy logic based sliding mode controlled dc-dc Boost converter," in *Electrical and Computer Engineering (ICECE), 2010 International Conference on*, 2010, pp. 70-73.

VITA

Yashwanth Chowdary Bezawada was born in Chilakakuripeta, Andhra Pradesh, India on the 25th December, 1992. He completed his bachelors in Electronics and Communication Engineering at Malla Reddy Institute of Technology and Science, Hyderabad India in 2014. He pursued his Master's degree at Old Dominion University on Electrical and Computer Engineering in 2017. He worked on Transient and Efficiency of Microgrid under the guidance Dr. Yucheng Zhang.